TITLE:

Hybrid local and distributed coding in PMd/M1 provides separation and interaction of bilateral arm signals

AUTHORS:

Tanner C. Dixon[1], Christina M. Merrick[4], Joni D. Wallis[1,2,4], Richard B. Ivry[1,2,4], Jose M. Carmena[1,2,3]

AFFILIATIONS:

1) UC Berkeley – UCSF Graduate Program in Bioengineering

2) Helen Wills Neuroscience Institute, University of California-Berkeley, Berkeley, CA 94720, USA

3) Department of Electrical Engineering and Computer Sciences, University of California-Berkeley, Berkeley, CA, 94720, USA

4) Department of Psychology, University of California-Berkeley, Berkeley, CA 94720, USA

CONTACT:

tcd44@berkeley.edu; jcarmena@berkeley.edu

ABSTRACT:

Pronounced activity is observed in both hemispheres of the motor cortex during preparation and execution of unimanual movements. The organizational principles of bi-hemispheric signals and the functions they serve throughout motor planning remain unclear. Using an instructed-delay reaching task in monkeys, we identified two components in population responses spanning PMd and M1. A 'localized' component, which confined activity within arm-specific sub-populations, emerged in PMd during preparation. It was most prominent following movement when M1 became strongly engaged, and principally involved the contralateral hemisphere. In contrast to recent reports, these localized signals solely accounted for divergence of arm-specific neural subspaces. The other 'distributed' component mixed signals for each arm within units, and the subspace containing it did not discriminate between arms at any stage. The statistics of the population response suggest two functional layers of the cortical network: one spanning hemispheres supporting preparatory and ongoing processes, and another specifying unilateral output.

INTRODUCTION

In the primate cortex, direct control of arm movement is primarily mediated by contralateral descending projections (Lawrence and Kuypers, 1968; Brinkman and Kuypers, 1973; Soteropoulos et al., 2011). However, numerous studies have observed activity changes in the motor cortex during movements of the ipsilateral arm (Matsunami and Hamada, 1981; Hoshi and Tanji, 2002; Carmena et al., 2003; Cisek and Kalaska, 2003; Ganguly et al., 2009; Ames and Churchland, 2019; Heming et al., 2019) and hand (Tanji et al., 1988; Verstynen et al., 2005; Diedrichsen et al., 2013). The functional role of this ipsilateral activity has been the subject of considerable debate, with hypotheses ranging from a role in postural support, bimanual coordination, or an extrapyramidal control signal for unimanual movements.

Neurons in the primate dorsal premotor cortex (PMd) play a critical role in motor preparation (Weinrich et al., 1984; Shen and Alexander, 1997; Hoshi and Tanji, 2002; Cisek and Kalaska, 2003). Interestingly, their response properties and degree of laterality appear to change across the course of preparation. For example, within PMd, individual units exhibit a transition from effector-independent to effector-dependent encoding between preparatory and execution phases of reaching. In contrast, primary motor (M1) units primarily become active during movement itself and show a pronounced contralateral bias (Cisek and Kalaska, 2003). This suggests a transition from abstract planning to explicit specification of motor output parameters in the signals of individual neurons. A similar transition has been shown in the activation of different cell-types from mouse premotor areas: In a directed licking task, neurons with intracortical projections displayed bilateral selectivity and dominated the population response early during planning, while neurons with descending output that drove movement were contralaterally biased and only became active closer to the time of movement onset (Li et al., 2015). These studies support the idea that pre- and primary motor areas may contain both a component for performing abstract computations, and an output component that is lateralized, reflecting precise details of the movement.

The classic perspective outlined above has been revisited in studies that focus on population-level analysis, considering instead how control might be reflected in the way the network coordinates activity. Low-dimensional representations of large-scale neural recordings can be used to characterize these patterns, revealing changes in the covariance structure across behavioral settings that are not evident when looking at single neurons in isolation (Cunningham and Yu, 2014). Ostensibly, these changes reflect reorganization of the population as it engages in different computational processes. When used to describe the changes between preparation and execution, pre-movement activity has been shown to evolve within an “output-null” subspace towards an optimal initial population state (Churchland et al., 2010; Kaufman et al., 2014; Elsayed et al., 2016). This initial state is advantageously positioned for engaging the internal dynamics of the network to produce patterned output for driving movement (Churchland et al., 2012; Shenoy et al., 2013; Sussillo et al., 2015). The bilateral, effector-independent activity observed in single neurons may support these preparatory and dynamic properties at the population level (Li et al., 2016).

While a bilateral network may support effector-independent functions, one would expect some form of effector-specific signaling as unimanual movements are prepared. There are two fundamental ways that population activity could specify the selected arm across preparation and movement. (1) Signals may localize within unique sub-populations for each arm (i.e., within hemispheres, brain areas, or cell types).

(2) Signals may be distributed across the same units yet maintain unique covariance structure that separates along arm-specific neural dimensions. Importantly, either of these architectures provides a way for downstream targets to discriminate signals and also yields the mathematical result of divergent subspaces. Arm-specific subspaces have been observed in the motor cortex during rhythmic movements (Ames and Churchland, 2019) and in response to joint perturbations (Heming et al., 2019). These studies suggest that the same neurons are involved during movement of either arm, and that separation of arm-specific signals is an emergent property of the population. However, past work in single-unit and cell-type specific physiology suggests that at least a portion of population activity is lateralized, particularly upon movement onset (Cisek and Kalaska, 2003; Li et al., 2015). This may suggest a simpler explanation for the presence of arm-specific subspaces, where separation of arm signals is a trivial result of strong localized encoding, and signals that are shared within units represent the parallel operation of distinct effector-independent processes.

In the present study, we investigated the extent to which population signals are localized within arm-specific sub-populations as movements are prepared and executed. Furthermore, we characterized the dependence of subspace separation on this signal localization at each stage, and tested whether signals that were mixed within units represented a shared subspace for the two arms or whether they contributed to subspace divergence.

We recorded large populations of single-units in PMd and M1 bilaterally while monkeys performed an instructed-delay unimanual reaching task. During preparation, activity began to localize within arm-specific sub-populations located primarily within contralateral PMd. This occurred despite many of the units being arm-neutral, as there was a strong tendency for arm-dedicated units to be more highly modulated. Following movement, M1 became more prominently involved and a larger proportion of the modulation in the population became localized. As a result, subspaces corresponding to the two arms diverged across the trial. We found no evidence that subspace separation was an emergent property of population-level analysis; rather, it reflected localized variance. However, we did observe behaviorally specific information that was shared at the level of single-units. The subspace in which this information was contained did not segregate signals for the two arms. Taken together, the results point to two primary components in the population response: (1) A localized component that develops across preparation, reaches a maximum during movement, and mirrors the lateralized anatomy of corticospinal output with its contralateral bias. (2) A distributed component representing a bilateral network that may support preparation and reflect internal dynamics of the evolving population state.

RESULTS

Behavior

Two macaque monkeys were trained to perform an instructed-delay reaching task in 3-D space (Figure 1A). Reaching movements were freely performed in an open area while kinematics were recorded using optical motion tracking. Visual feedback of endpoint position and task cues were provided through a virtual 3-D display. Each trial had three phases (Figure 1B). For the Rest phase, the monkey placed both hands in start targets positioned near the torso and remained still for 500 ms. For the Instruct phase, an instructional cue appeared at one of six target locations. The color of the cue specified the required hand for the forthcoming trial. The monkey was required to keep both hands in the rest positions while the cue remained visible for a variable interval (500 – 1500 ms). The Move phase was initiated when the

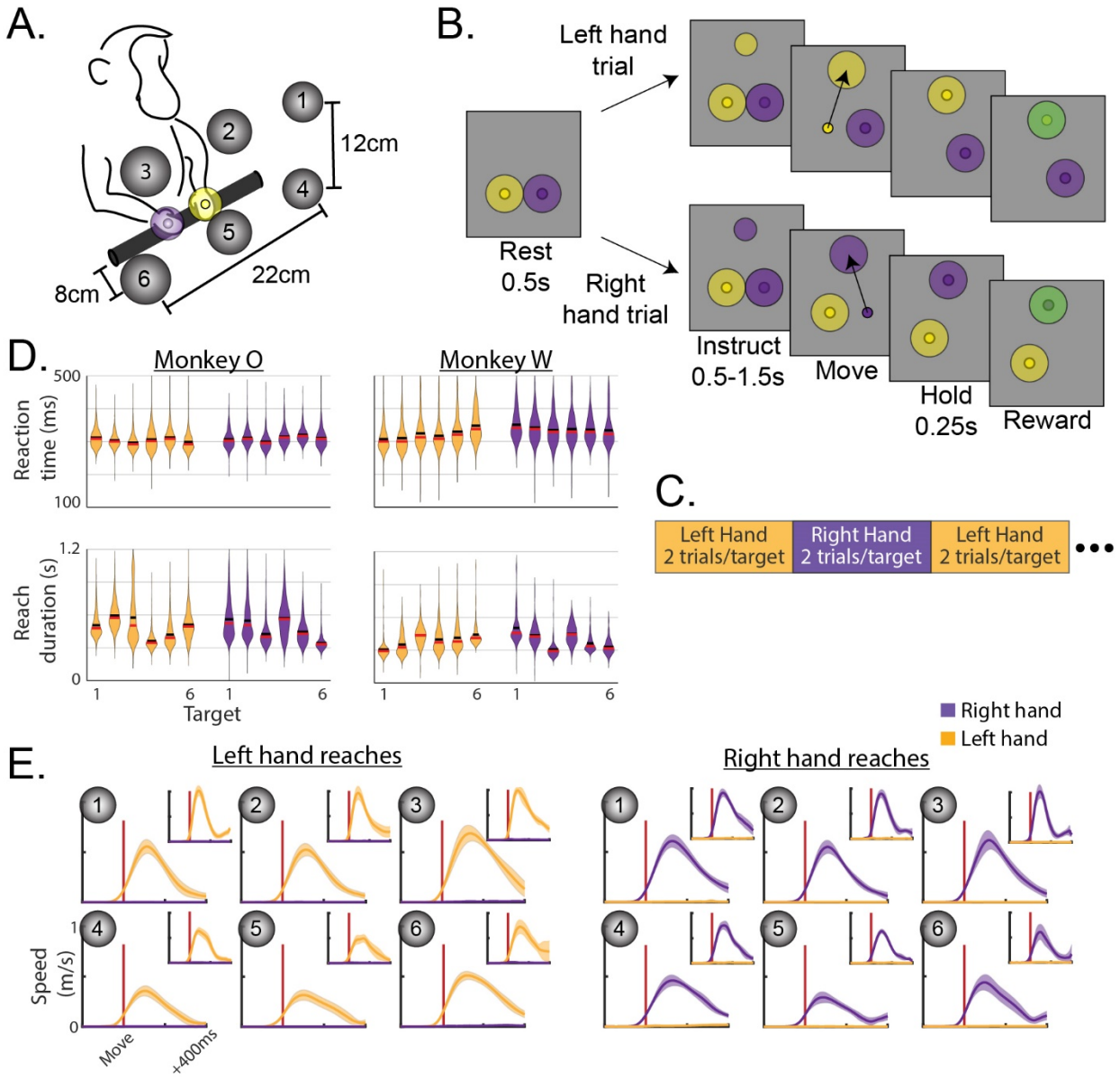

Figure 1. Behavior.

(**A**) Monkeys reached to one of six virtual targets, indicated by grey spheres in the cartoon. During the task these would be invisible until one appeared to instruct the reach. (**B**) Trials consisted of 3 phases. Each trial was initiated by placing both hands in start targets and remaining still for 500ms ('Rest' phase). A small target then appeared at the location of the future reach in a color that indicated which hand to use. The monkey remained still during cue presentation for 0.5-1.5s ('Instruct' phase). The start target for the reaching hand then disappeared while the reach target enlarged to cue movement ('Move' phase). (**C**) Hand assignments followed a blocked schedule. (**D**) Distributions of reaction times (top row) and reach durations (bottom row) for each monkey, hand, and target. Left hand reaches in yellow, right in purple. Horizontal black bars show means, red bars show medians. (**E**) Speed profiles during left- or right-hand trials. Both reaching and stationary hands are plotted in each, although stationary speeds are near 0 and hardly visible. Vertical red lines indicate threshold crossing to mark movement onset. Monkey O main, monkey W inset. Mean +/- standard deviation.

start position marker for the reaching hand disappeared and the cue at the target location increased in size, which signaled the animal to reach. The monkey received a juice reward if it accurately reached the target and maintained the final position for 250 ms, while keeping the non-cued hand at its start position for the duration of the trial. 300ms representative windows from each phase were used in data analysis. Trials were blocked for each arm, alternating 2 trials per target for the left arm, then 2 trials per target for the right (Figure 1C).

Average success rates were above 95% for both hands in both monkeys. Overall, reaction times averaged 308 ms for monkey O and 333 ms for monkey W. Distributions of reaction times for each hand/target combination are displayed in Figure 1D, which were fairly consistent across the workspace. Reach biomechanics varied across the workspace, resulting in slightly different reach durations across targets (Figure 1D). In terms of kinematics, the initial feed-forward portions of reaches were smooth and stereotyped (Figure 1E). There was a very slight but significant increase in the speed of the non-reaching hand between Rest (mean – monkey O: 1.1 mm/s; monkey W: 2.9 mm/s) and Move (mean – monkey O: 3.6 mm/s; monkey W: 7.6 mm/s) phases of the task (permutation test – monkey O: p=1.0e-4; monkey W: p=1.0e-4). We note that the task was designed to mimic natural reaching without the use of physical restraints. As such, we assume the small movements in the non-reaching arm are part of the normal behavioral repertoire occurring during natural unimanual reaching. Nonetheless, we will address any reasonable impacts these small movements may have in our neural analyses.

Arm-dedicated units emerge across task phases while the majority remain arm-neutral

We recorded 433 and 113 single-units in the caudal aspect of dorsal premotor cortex (PMd) in monkeys O and W, respectively, and 331 and 289 single-units in primary motor cortex (M1) (Figure 2). Since both arms were used in the behavior, we can evaluate the ipsi- and contralateral response in each unit. Units were pooled across hemispheres in the analysis, with 'Contralateral' summaries reflecting the collection of responses during trials performed with the contralateral arm, and vice-versa for trials performed with the ipsilateral arm. PMd and M1 units were analyzed separately. Firing rates were soft-normalized using the Rest phase mean and standard deviation, and modulation strength is expressed as the mean squared value of these standard scores within the window of interest.

We first analyzed single units to determine the degree of modulation during the Instruct and Move phases of the task (Figure 3). Following instruction, many units in both PMd and M1 became significantly modulated for movements of one or both arms (Table S1). Units in PMd were, on average, more strongly modulated during the Instruct period than those in M1 (Figure 4A; permutation test – monkey O: p=0.012; monkey W: p=3.2e-3). This relationship reversed following movement, with average modulation in M1 becoming stronger than PMd (Figure 4A; permutation test – monkey O: p=2.6e-3; monkey W: p=0.012). These results are in line with the view that PMd plays a privileged role in motor preparation. The distributions of modulation values were heavy-tailed and contained some notably extreme values; however, we chose not to apply any outlier criteria. Controls are performed later in our population-level analyses to ensure that results are representative of trends across the entire population rather than a few extreme units.

We next considered the laterality of each unit by quantifying the relative modulation observed during ipsi- and contralateral trials. We expressed each unit's arm preference on a scale from -1 to 1, with 1 indicating exclusive contralateral modulation and -1 indicating exclusive ipsilateral modulation (Figure

4B). Although the cue for the forthcoming trial had yet to be presented during the Rest phase, arm selection could be implied from the blocked task structure (Figure 1C). However, except for a very small effect in PMd of monkey O (one-sample t-test – μ_{Rest}=0.06, p=9.7e-5), there was no significant contralateral bias observed during the Rest phase in either brain area for both monkeys. Despite the lack of contralateral bias, both monkeys entered arm-specific population states during the Rest phase, which was more pronounced in PMd populations (mean difference between left and right arm firing rates – monkey O PMd: 1.85Hz, M1: 1.64Hz; monkey W PMd: 1.33Hz, M1: 0.98Hz; Figure 4C). For trials in which the same hand was repeated from the previous trial only, it was possible to classify the hand for the forthcoming movement from the population activity (Figure S1).

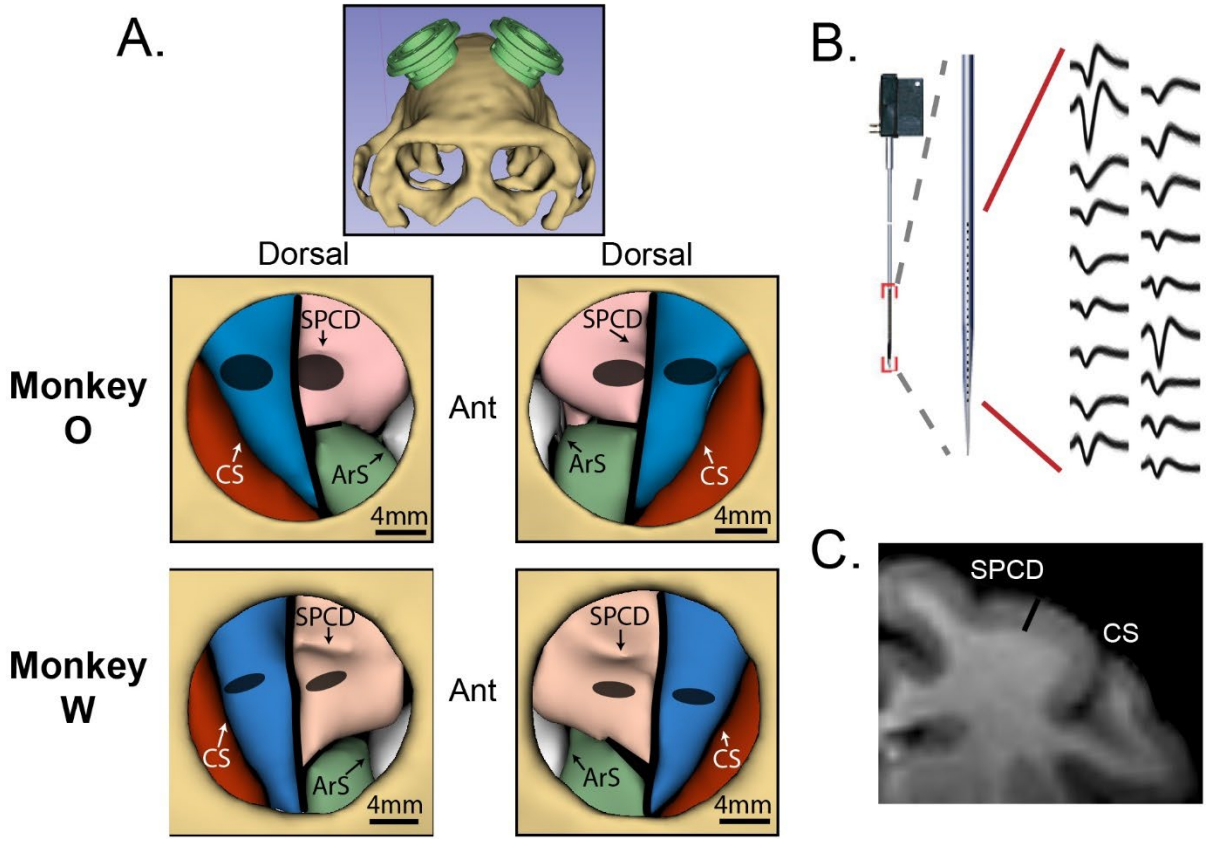

Figure 2. Neural recordings.
(**A**) MRI-based volume renderings of the skull and target brain regions. Top panel shows the arrangement of the two chambers. Two bottom rows show segmented brain regions within the cranial window of each chamber, for each monkey. Region boundaries were assigned based on Paxinos et al., 2009. Red - somatosensory cortex; blue - primary motor cortex (M1); pink - dorsal premotor cortex (PMd); green - ventral premotor cortex; white - frontal eye field. CS - central sulcus; SPCD - superior pre-central dimple; ArS - arcuate sulcus. Grey ellipses indicate regions sampled by recordings. (**B**) Interlaminar recordings were obtained using V- and S- probes (Plexon, Inc., Dallas, TX) with 24-32 electrodes aligned perpendicular to the cortical surface. Example waveforms were all simultaneously recorded from a single probe. (**C**) MRI coronal slice, monkey O. 3mm black bar is approximately equal to the distance spanned by electrodes on 32-channel probes. Same landmark labels as in (**A**).

The emergence of laterality after the onset of the instruction cue mirrored the emergence of general unit modulation: A contralateral bias was present in PMd during the Instruct phase and then became present in both PMd and M1 during movement. Mean arm preference in PMd showed a modest but significant bias in the contralateral direction during the Instruct phase (one-sample t-test – monkey O: $\mu_{Instruct}$=0.11, p=7.0e-8; monkey W: $\mu_{Instruct}$=0.16, p=1.8e-4) and showed no significant change between Instruct and Move (paired-sample t-test – monkey O: μ_{Move}=0.15, p=0.11; monkey W: μ_{Move}=0.13, p=0.65). Mean arm preference in M1 did not show a significant contralateral bias until the Move phase (one-sample t-test – monkey O: $\mu_{Instruct}$=0.03, p=0.13; μ_{Move}=0.07, p=0.013; monkey W: $\mu_{Instruct}$=0.02, p=0.31; μ_{Move}=0.20, p=5.1e-11).

While shifts in the means were modest, changes in arm preference across phases were most evident in the emergence of a subset of units that strongly preferred one arm or the other (Figure 4C). These arm-dedicated units typically preferred the contralateral arm, demonstrated by increased occupancy in the contralateral tails of the arm preference distributions; however, a small proportion of the population was exclusively modulated during ipsilateral trials as well (Figure 4B). Despite much of the population remaining arm-neutral (arm preference near 0) or preferring the ipsilateral arm, the emergence of strongly contra-dedicated units was sufficient to drive contralateral shifts in the population mean. In summary, despite much of the population remaining arm-neutral, an increasing number of highly arm-dedicated units emerged with each task phase, primarily favoring the contralateral arm.

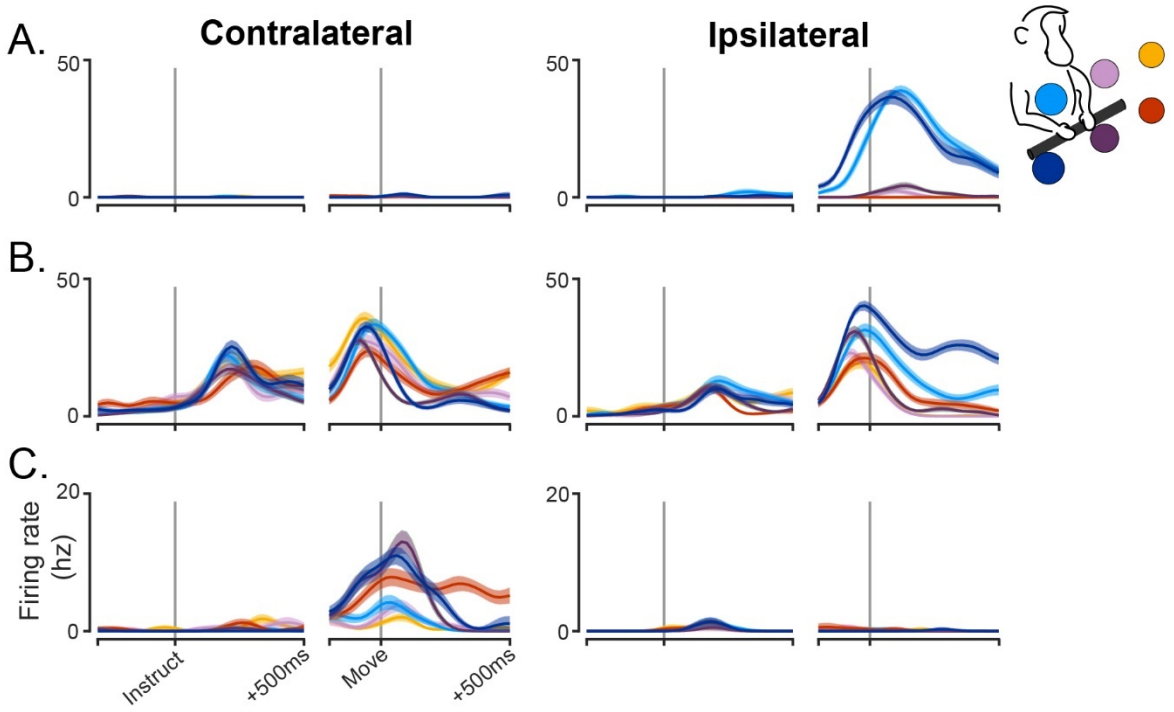

Figure 3. Firing rate traces of example single-units.

Trial-averaged firing rates for 3 example single-units, all from the left hemisphere. Each color represents a different target according to the color-coding in the top right. Mean +/- SEM. (A) An M1 unit exclusively modulated during ipsilateral movements. (B) A PMd unit with both Instruct and Move phase modulation for both arms. (C) A PMd unit with modest contralateral modulation during the Instruct phase and strong contralateral modulation during movement, but no modulation on ipsilateral trials.

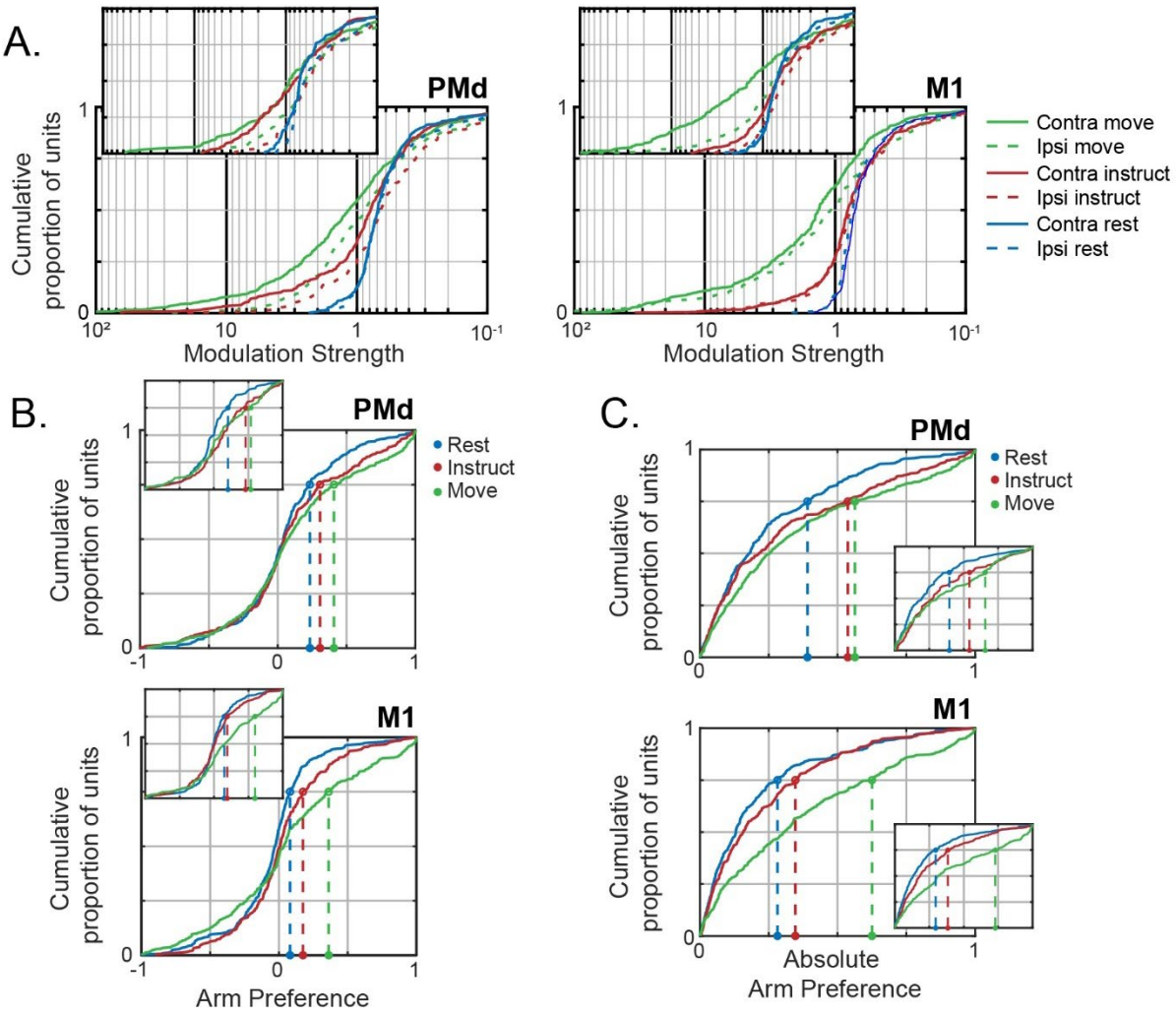

Figure 4. An increasing number of arm-dedicated units emerge with each task phase.
(**A**) Cumulative distribution of single-unit modulation during each phase, arm. Left panel PMd, right panel M1. Large values cut off by plot: monkey O Contra Move [134(PMd), 133(PMd), 104(PMd)], Ipsi Move [234(M1), 181(M1), 130(M1)]; monkey W Contra Move [125(M1)]. (**B**) Cumulative distribution of arm preferences during each phase. Top panel PMd, bottom panel M1. Negative values are ipsi-preferring, positive values are contra-preferring. Circles and vertical dashed lines mark the upper quartile of each distribution (**C**) Same as (B), but using the absolute value of arm preference to indicate arm dedication, independent of hemisphere. For all plots: monkey O main, monkey W inset.

230 Modulation preferentially occurs within arm-dedicated units

231 There are two primary means by which population signals can specify the selected arm at each phase.
232 (1) Arm-neutral units may maintain unique covariance structure for each arm that separates signals
233 along different neural dimensions at the population level. (2) Arm-dedicated units may dominate the
234 population response, thereby representing the majority of population variance in dedicated sub-
235 populations. The latter possibility is investigated over the following two sections. First, we consider
236 whether modulation preferentially occurs in units that are strongly dedicated to one arm or the other.

237 We performed a regression analysis to quantify the relationship between strength of arm preference
238 and modulation for the preferred arm. Importantly, arm preference and modulation were calculated
239 from independent data sets so that there is no mathematical linkage between the two measures when
240 assessing their relationship. A slope of 1 corresponds to an order of magnitude increase in modulation,
241 on average, when comparing perfectly arm-neutral units with fully arm-dedicated units. As seen in
242 Figure 5A, the slopes are initially near zero and then become positive over time. To quantify these
243 changes, we used a multi-factorial permutation approach to test for effects of Area (PMd, M1), Phase
244 (Rest, Instruct, Move), and Preferred Arm (Ipsi, Contra) on the population slopes.

245 We found a main effect of Phase in both animals (monkey O: p=1.0e-4, monkey W: p=1.0e-4): a positive
246 correlation between arm preference and modulation strength emerged and strengthened across task
247 phases (Figure 5A-B). By the Move phase, there was approximately a ten-fold increase in the modulation
248 strength of arm-dedicated units when compared to arm-neutral units. Since PMd displayed greater
249 modulation than M1 during preparation but not movement, we tested whether the two areas had
250 differing slopes in each phase independently. We found a significant simple effect of Area during the
251 Instruct phase (monkey O: p=3.0e-4; monkey W: p=6.3e-3) but not the Move phase (monkey O: p=0.13;
252 monkey W: p=0.91). Thus, the relationship was more prominent within PMd prior to movement, while
253 the two areas became roughly equivalent following movement initiation. This was confirmed with a test
254 for 2x2 interaction (monkey O: p=0.025; monkey W: p=9.9e-3).

255 Given the overall contralateral bias, we further tested whether this relationship held for both contra-
256 and ipsi-preferring units. For the contra-preferring units, there was a significant simple effect of Phase
257 (monkey O: p=1.0e-4; monkey W: p=1.0e-4). For the ipsi-preferring units, the Phase effect was
258 significant for monkey O (p=1.0e-4), but only trended in this direction for monkey W (p=0.087), perhaps
259 due to the lower amount of ipsilateral modulation in monkey W. Slopes were generally steeper for
260 contra-preferring units. The simple effect of Preferred Arm was significant during the Instruct phase for
261 both monkeys (monkey O: p=0.033; monkey W: p=1.0e-4), and significant for Monkey W during the
262 Move phase (monkey O: p=0.53, monkey W: p=1.0e-4). Given that there are also more contra-dedicated
263 units than ipsi-dedicated units, these results suggest that a larger proportion of the contralateral signal
264 was localized within dedicated sub-populations compared to the ipsilateral signal. We directly test this
265 conjecture in the following section where we consider population-level implications of these results.

266

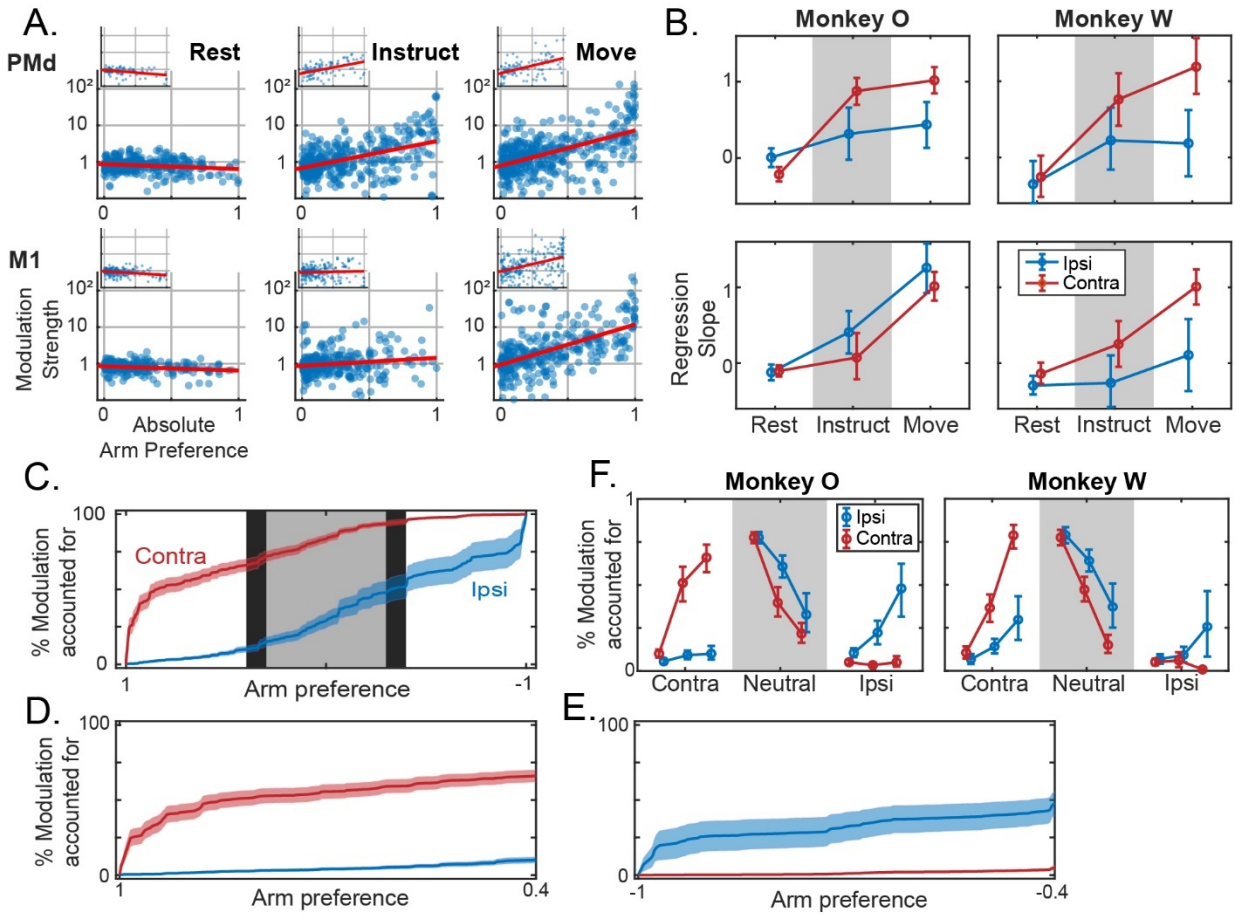

Figure 5. Neural activity is progressively consolidated within arm-specific subpopulations. (**A**) Modulation for the preferred arm plotted against arm preference, for all units in each brain area and task phase. Log-linear best fit lines are displayed in red. Inset figures belong to Monkey W. (**B**) Slopes of regression lines fit to data from (A), independently for ipsi- and contra-preferring sub-populations. Mean +/- bootstrapped 95% confidence interval. (**C-E**) For the move phase in monkey O, cumulative modulation plotted against arm preference, i.e. each point indicates the proportion of modulation accounted for by all units with arm preference values to the left of the indexed position. Positive values on the x-axis indicate contra-preferring, and negative values indicate ipsi-preferring. Shaded error bars indicate bootstrapped standard error. (**C**) The full spectrum of arm preferences is shown. Shaded backgrounds indicate three partitions: Contra-dedicated [0.4, 1] and Ipsi-dedicated [-1, -0.4] in white, and Neutral [-0.3, 0.3] in grey. (**D**) Cumulative modulation within contra-dedicated regime. (**E**) Same as (D), but ipsi-dedicated. Note inverted axis. (**F**) The proportion of modulation within each partition from (C) during ipsi- or contralateral movements. Note that the total modulation is significantly lower for ipsilateral movements, particularly for Monkey W, and these data are only displayed as proportions. Mean +/- bootstrapped 95% confidence interval.

283 The population signal is largely confined to arm-specific sub-populations
284 The preceding analyses establish that there is an increase across task phases in the proportion of units
285 that are strongly dedicated to a single arm, and that those units exhibit much more modulation in
286 activity relative to arm-neutral units. This suggests that the population signal is progressively
287 consolidating within arm-specific sub-populations even though many of the units remain arm-neutral.
288 To visualize the segregation of overall modulation, we ordered all units based on arm preference and
289 calculated their cumulative modulation (Figure 5C-E). Since PMd and M1 showed similar relationships in
290 the previous analyses, we combined units from the two areas, analyzing them as a collective population.
291 In the extreme case that population signals are entirely segregated, 100% of ipsilateral modulation
292 would occur at an arm preference of -1, and 100% of contralateral modulation would occur at +1.

293 We focused on two core questions. (1) Does the proportion of dedicated modulation increase across
294 task phases, indicating a progression towards independent signals? (2) Does the amount of independent
295 (or dedicated) modulation differ for ipsi- and contralateral activation? As expected, dedicated sub-
296 populations emerged that contained a large proportion of the modulation associated with movements
297 of one arm and only a small proportion of the modulation associated with the other arm (Figure 5C-F).
298 For statistical testing, we split the arm preference domain into 3 equal width regimes, corresponding to
299 contra-dedicated (arm preference > 0.4), ipsi-dedicated (arm preference < -0.4), and arm-neutral (-0.3 <
300 arm preference < 0.3) units, and summarized the data by expressing the proportion of modulation
301 contained within each regime (Figure 5F). We again used a multi-factorial permutation approach to test
302 for effects of Phase (Rest, Instruct, Move), and Arm (Ipsi, Contra). We will refer to ipsilateral modulation
303 in the ipsi-dedicated units simply as 'ipsi-dedicated modulation' and vice-versa for contra-.

304 For both animals, the effect of Phase was significant in the contralateral responses (p=1.0e-4/1.0e-4),
305 with the proportion of contra-dedicated modulation increasing across phases (Figure 4F, red lines). Ipsi-
306 dedicated modulation increased across task phases for both monkeys as well (Figure 4F, blue lines),
307 although this effect was only significant for monkey O (p=9.0e-4; monkey W: p=0.31). There was a
308 significant interaction between Arm and Phase for both monkeys (monkey O: p=1.0e-4; monkey W:
309 p=1.0e-4), indicating the stronger emergence of contra-dedicated modulation as compared to ipsi-
310 dedicated modulation. Both animals showed a simple effect of Hand during the Instruct phase (monkey
311 O: p=1.0e-4; monkey W: p=1.0e-4), with more contra-dedicated modulation being observed than ipsi-.
312 This effect was also significant during the Move phase for monkey W (p=1.0e-4) and approached
313 significance for monkey O (p=0.056).

314 These results suggest that arm signals consolidate within exclusive sub-populations throughout
315 preparation. Moreover, contralateral signals are more independent than ipsilateral signals, in the sense
316 that a larger proportion of the contralateral modulation was represented in contra-dedicated units.
317 Importantly, this characterization of the population response captures most of the modulation for each
318 arm in mutually exclusive sub-populations, which we will refer to as the 'localized' component. It is
319 important to emphasize that these sub-populations are not fully localized in terms of brain area or
320 hemisphere. While units that were dedicated to a single arm were typically located in the contralateral
321 hemisphere, some were located in the ipsilateral hemisphere and in both PMd and M1. Returning to the
322 possibilities outlined at the beginning of the previous section, we therefore conclude that the dominant
323 characterization of the population response is this localized component – dominant in the sense that it
324 represents the majority of modulation across the population.

Neural subspaces for the two arms diverge across task phases

We next sought to characterize the time course of changes in neural subspaces as movements were prepared and executed. We hypothesized that localized activation would drive population signals into diverging subspaces for the two arms. For these analyses, we pooled units from the left and right hemispheres. Using PCA, we first estimated the dimensionality of the neural subspace during each task phase using a cross-validated data reconstruction method (see Methods; Yu et al., 2009). This is an essential step to avoid drawing conclusions based on noise-dominated dimensions. Dimensionality was calculated separately for each session and arm. During Rest, the dimensionality was approximately 5-6, and decreased to approximately 4 during the Instruct and Move phases (Figure 6A). We therefore opted to focus on only four components to represent the neural subspaces of each dataset.

We calculated the alignment between PCA subspaces associated with left or right arm movements using a metric that describes the proportion of low-dimensional variance for one dataset that is captured in the low-dimensional space of another (see Methods; Athalye et al., 2017). If the network is organizing activity in the same way across datasets, then the covariance alignment is 1, regardless of signal magnitude. If activity is reorganized into orthogonal subspaces across datasets, then the covariance alignment is 0. Two types of alignment measurements were made: (1) Subspaces were fit to random partitions of trials for the same arm – what we will refer to as 'native' alignment – giving us an estimate of natural variability in our subspace estimates when compared over the same time window, and describing the evolution of the motor plan when comparing across time windows. (2) Subspaces were fit separately using trials for either arm and compared with each other – what we will refer to as 'cross' alignment – describing the divergence of the subspaces for the two arms at each task phase.

Using single-trial activity event-locked to the onset of instruction and movement, we were able to capture the fine-timescale evolution of any emerging or diverging subspaces (Figure 6B-C). When comparing the native alignment across task phases, we observed the emergence of distinct Instruct and Move period subspaces. Figure 6B shows these data displayed as a continuous heat map with block diagonal structure that coincides with the phase transitions. Within each phase native alignment was high, indicating consistent low-dimensional structure in the population activity that was specific to each stage (Figure 6B; Figure 6D filled circles).

As expected, subspaces for the two arms gradually diverged across task phases (Figure 6C; Figure 6D open circles). On the whole, subspaces for the two arms were significantly less aligned than the (cross-validated) comparisons within the same arm (Figure 6D open vs filled circles; two-way ANOVA, ME comparison type – monkey O: p=7.8e-68; monkey W: p=4.2e-37). Interestingly, subspace divergence was already apparent during the Rest phase (paired sample t-test, native-Rest vs cross-Rest – monkey O: p=1.2e-15; monkey W: p=1.3e-10). As mentioned in our analysis of single-unit arm preferences, this is likely due to predictable arm assignments from the blocked task structure (Figure 1C, Figure S1). Cross alignment decreased significantly as the trial unfolded, reaching a minimum during movement (one-way repeated measures ANOVA – monkey O: p=1.4e-7; monkey W: p=5.9e-8). These results map closely onto the progressive localization described in the previous section.

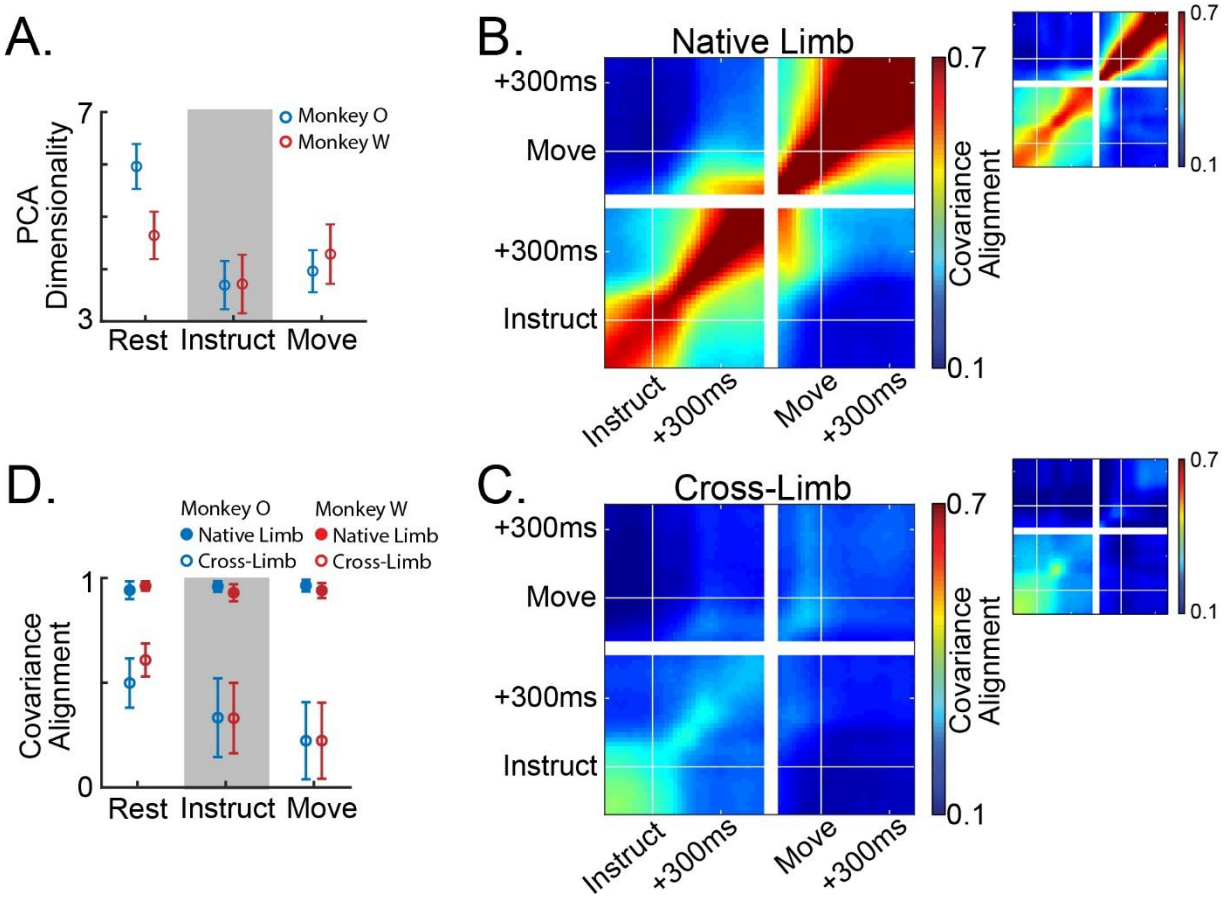

Figure 6. Population activity reorganizes and diverges for the two limbs throughout planning. (**A**) Dimensionality of the PCA subspace estimated as the number of components that minimizes the cross-validated reconstruction error of the full-dimensional neural data. Mean +/- standard error across datasets. (**B,C**) Heat maps indicate alignment of 4-dimensional PCA subspaces between all pairs of timepoints across the Instruct and Move phases of the task, averaged across sessions. (**B**) Compares subspaces across time for movements of the same arm. Three blocks forming along the diagonal indicate three distinct subspaces: a pre-instruction 'Rest' space, a post-instruction 'Instruct' space, and a peri-movement 'Move' space. (**C**) Compares subspaces across time for movements of opposite arms. Prior to instruction there is a moderate alignment of the subspaces for each limb, however, the two subspaces diverge around 100ms post instruction. (**D**) Summary of the data in (B,C). Mean +/- standard deviation across datasets.

Subspace separation relies upon localized signals

Activity within mutually exclusive sub-populations naturally separates into distinct linear subspaces; as such, we can expect some level of subspace separation as a simple result of variance in arm-dedicated units. However, it is possible that subspace separation could occur within a distributed representation as well (Ames and Churchland 2019; Heming et al, 2019). This question is especially important in considering arm-neutral units. Even though these units, by definition, show similar levels of activity during contra- and ipsilateral movement, it is possible that their population-level contributions are different for these two types of movements, and thus also contribute to subspace separation.

To investigate the extent to which subspace separation relied upon localized activation, we analyzed the structure of PCA subspaces via their coefficient weights. Since components of PCA models form an orthogonal basis set, each can be independently analyzed to determine its contribution to subspace divergence. We fit separate PCA models for each arm and task phase and calculated two statistics for each component: (1) To capture the contribution of a given component to subspace separation, we calculated the ratio of variance it captured for the two arms (right/left). (2) To capture the dependence of a given component on arm-dedicated units, we calculated a coefficient-weighted average of the arm preferences for all units (e.g., if non-zero weights were only given to right arm dedicated units, this value would be 1; if weights were evenly distributed across the spectrum of arm-preferences, this value would be 0). A strong relationship between these two metrics would suggest that subspace separation relies upon localized activation.

Indeed, this was the case during both the Instruct and Move phases. Figure 7A-C shows a single session example from the Move phase. The top principle components captured a large amount of the variance for the left arm while capturing little variance for the right arm. Components with a variance ratio strongly favoring the left arm almost exclusively weighted units that were themselves highly dedicated to the left arm. The lower components with more balanced variance ratios distributed weights more evenly across the arm preference spectrum. This pattern was evident in each phase throughout recordings from both monkeys. Figure 7D shows the relationship between right/left variance ratio and coefficient-weighted arm preference for the top five principal components of each dataset. Following the instruction cue, components that strongly discriminated between the two limbs (variance ratio far from 1) primarily weighted units that were themselves highly discriminating. This relationship remained strong as the range expanded during the Move phase. The same pattern was observed when firing rates were normalized using an alternative method to avoid overrepresentation of highly modulated units (Figure S2A). In summary, these results suggest that the subspace separation described in the previous section relies upon unit-level signal localization.

Additional distributed signal contains behaviorally specific information about both arms

The preceding sections make clear that the population signal is dominated by a localized organization. Nonetheless, it is likely that the arm neutral units also provide a meaningful distributed component, one that coexists with the localized one. These units may contain behaviorally specific information that is obscured by the high magnitude localized signal when analyzing the population response at large. To test this hypothesis, we divided the entire population of units from both hemispheres and brain areas into two subgroups based on the preferred arm of each unit from a held-out dataset (Figure 8A). If the signals are entirely localized, each sub-population would only contain information about its preferred

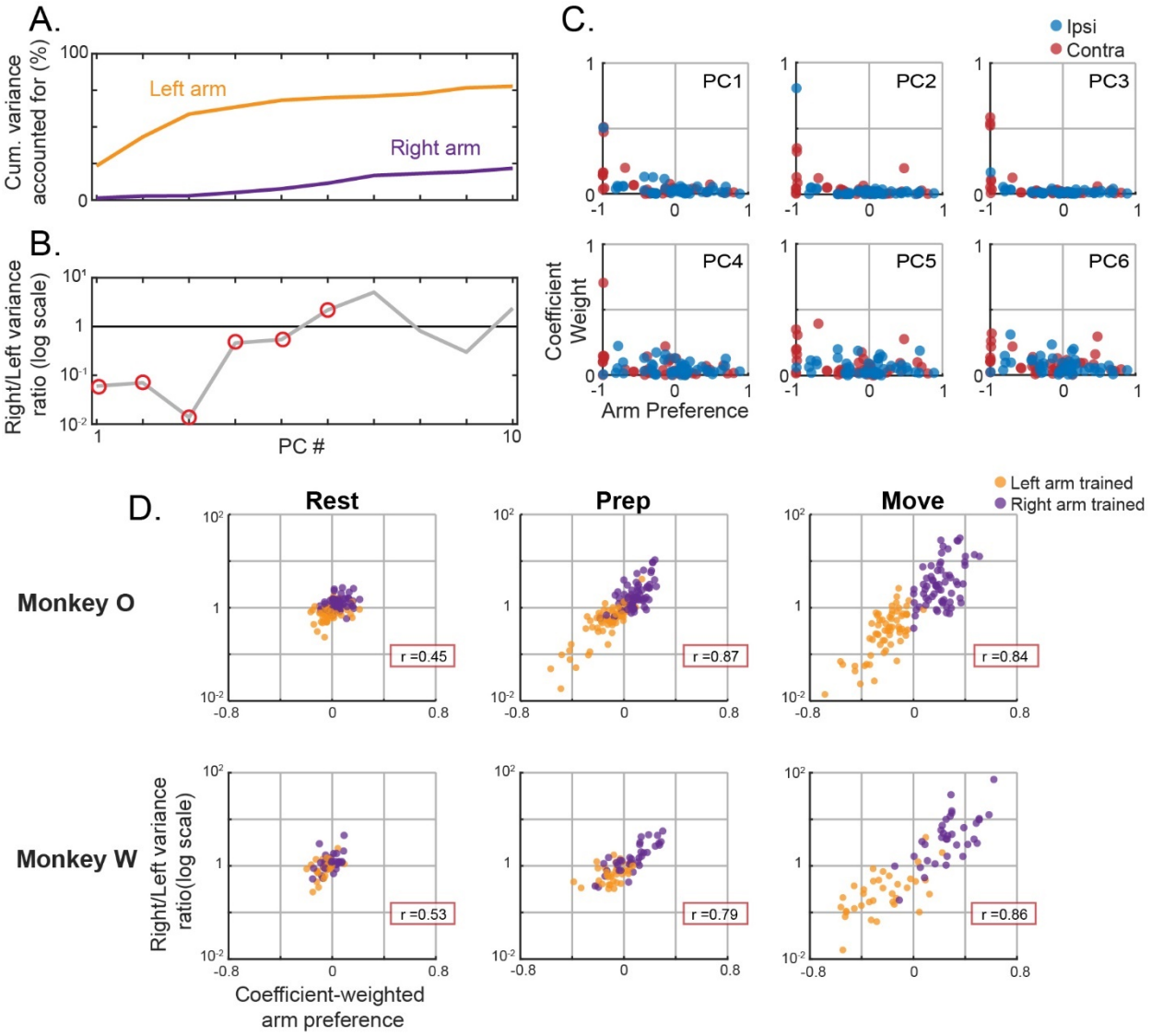

Figure 7. Separation of arm-specific subspaces relies upon unit-level segregation.
(**A-C**) Single session example of a PCA model trained to capture bi-hemispheric activity during left arm movements. Held-out testing data for 86 simultaneously recorded units were used. (**A**) Cumulative proportion of variance accounted for across the top 10 principal components. (**B**) For each component, the ratio of the explained variance between the two limbs. (**C**) Absolute values of the coefficient weights for each component plotted against the corresponding unit's arm preference. Top row represents components 1-3; bottom row represents components 4-6. Positive arm preference values indicate right arm preferring units. (**D**) The component variance ratio for the two arms plotted against a coefficient-weighted average of the arm preferences for each unit in that component. Datapoints represent the top 5 principal components of left or right arm trained models across all sessions. Separate models for each phase are plotted in each column. Pearson correlation coefficient for each dataset is displayed in the red box. Top row monkey O, bottom row monkey W.

arm (e.g., a left arm-preferring sub-population would be predictive of left but not right arm movements). However, if there is some amount of distributed coding, then each sub-population will contain both localized and distributed information about its preferred arm, but only distributed information about its non-preferred arm.

We first analyzed the time course of modulation for each sub-population during movements of the preferred and non-preferred arms. While modulation during preferred-arm trials was much stronger in the Instruct and Move phases, there was a small amount of modulation during trials of the non-preferred arm as well (Figure 8B). To determine whether this modulation carried precise information about the behavior, and not just non-specific changes related to task engagement or small movements of the non-selected arm, we trained linear discriminant analysis (LDA) classifiers to predict the target on each trial. Even though the units showed very little modulation when the non-preferred limb was used, prediction accuracy was above chance (Figure 8C-E, paired sample t-test with Rest – monkey O: Instruct p=1.5e-12, Move p=4.1e-21; monkey W: Instruct p=1.8e-3, Move p=1.1e-7). This suggests that the population code is not entirely localized but contains a meaningful distributed component as well. We refer to this as 'distributed' in the sense that the contributing units reflect information about both arms.

Distributed code is contained in a shared subspace for the two arms

We next asked whether subspace separation exists specifically within the distributed portion of population activity. This is a non-trivial question given that localized activity dominates the population response in terms of explained variance. We again partitioned the population based on preferred arm and fit 4-D PCA models to the neural activity obtained from trials in which the movement was produced by the non-preferred arm. This is a conservative approach for capturing only the distributed signals, since localized activity will be absent during reaches of the non-preferred arm. We will refer to the subspace spanned by these models as the 'distributed' subspace.

Having isolated the distributed population structure, we can project neural data from both preferred and non-preferred arm trials onto this subspace and compute the amount of variance captured for each arm. If there is meaningful separation of arm-specific subspaces, then the activity of the preferred arm would be largely in the null space of this projection. We would therefore expect the distributed subspace to capture more variance (as a raw measure, not proportion of total) during trials of the arm it was fit to (the non-preferred arm). Alternatively, if the distributed signal exists within a shared subspace for the two arms, then the patterns of activity for either arm would be preserved through the projection, and we should expect as much or more variance captured for the preferred arm.

Across all task phases and for both animals, more variance was accounted for during preferred arm trials than during non-preferred arm trials (Wilcoxon signed rank – $p<0.05$ for all six comparisons). Variance ratios (expressed as non-preferred over preferred) were below 1 for nearly every individual dataset and became even lower with each subsequent phase (Figure 8F). We note that a lower ratio does not precisely mean "more shared variance," but rather, "more evidence against being unique." We again used an alternative firing rate normalization method to confirm that this result was not dependent on overrepresentation of units with the strongest modulation (Figure S2B). In summary, the subspace capturing distributed activity is not unique to the arm it was fit to, but rather represents a shared subspace for population activity associated with either arm.

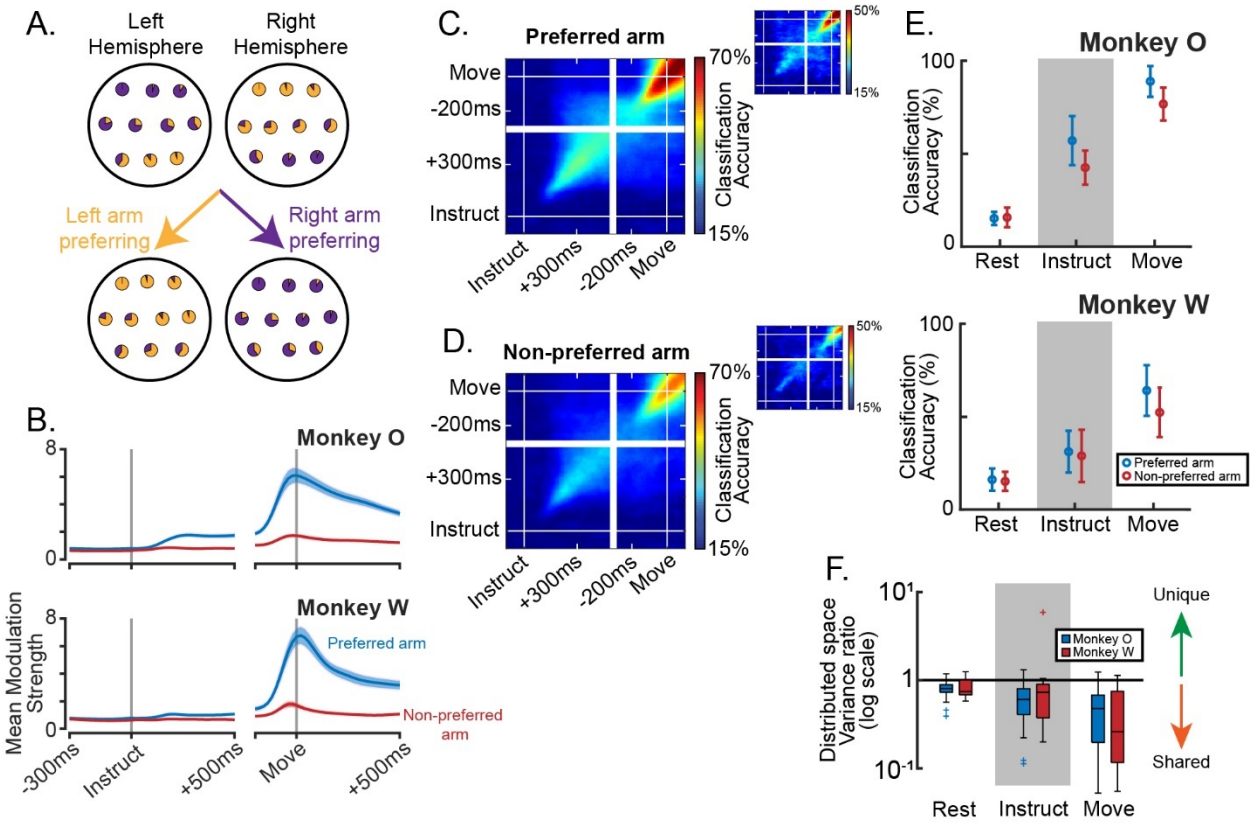

Figure 8. Behaviorally specific information exists within a subspace that captures bilateral activity. (**A**) Illustration of the population partitioning approach. Each unit is represented as a pie-chart displaying the relative modulation during left and right arm trials. Most units in the left hemisphere are more strongly modulated during right arm movements (mostly purple pie-charts), yet some prefer left arm movements (mostly yellow pie-charts). Regardless as to which hemisphere each unit is in, the population may be subdivided into left and right arm preferring sub-populations. On the extreme that all information about each arm is contained within dedicated sub-populations, this simple division will fully segregate the signals such that movements of the non-preferred arm cannot be classified. (**B**) Modulation as a function of time, taken as the mean over all units during trials of their preferred or non-preferred arm, +/- standard error. (**C**) Target classification accuracy using LDA for movements of the preferred arm. Models are trained on each time point and tested on each time point to provide high temporal resolution and inform cross-phase generalization of the classifier. Plots are averaged over all sessions (13 Monkey O, large plots; 7 Monkey W, small plots) and both sub-populations (left-preferring, right-preferring). (**D**) Same as (C), but for non-preferred arm movements. (**E**) Summary data of (C,D) for monkey O, top panel, and monkey W, bottom panel. Mean +/- standard deviation across datasets. (**F**) Ratio of the variance captured in the distributed subspace for the two limbs.

DISCUSSION

We have shown that the combined population response spanning PMd and M1 across hemispheres contains two primary components. The first is supported by unique sub-populations representing each arm primarily, but not entirely, within the contralateral hemisphere. This component first emerged within PMd after instruction and became most prominent during movement when M1 became strongly engaged. Despite much of the population being arm-neutral, there was a bias for stronger modulation within arm-dedicated units. The majority of modulation was therefore localized within units that were devoted to one arm or the other. This localized organization resulted in trivial separation of the neural subspaces associated with movements of each arm. We also found a second component that leveraged shared signaling within units. This component was much smaller in magnitude but contained behaviorally specific information that could be used to accurately classify reaching targets. In contrast to the natural separability of the localized component, this distributed component mixed signals for the two arms within the same subspace.

Progressive localization of arm-dedicated signals

To our knowledge, this study is the first to compare low-dimensional population structure during preparation of left vs right arm reaching. It has been proposed that neural subspaces reorganize between preparation and execution of reaching movements (Elsayed et al., 2016). Given that previous studies have reported increases in the number of lateralized units during the transition from preparation to movement (Cisek and Kalaska, 2003; Li et al., 2015), we thought that activity may consolidate into arm-specific sub-populations, primarily in the contralateral hemisphere, as the population reorganizes between task phases. This would result in localized representations of the two arms, in the sense that each sub-population is primarily active only during movements of its respective arm. However, it has been recently proposed that even during active behavior, signals for the two arms are mixed at the level of single-units (i.e. distributed representation) but separate into unique linear subspaces (Ames and Churchland, 2019; Heming et al., 2019). The only clear separation of arm-specific signals that we observed during any phase occurred at the single-unit level (Figure 5). We found no evidence that signal separation was an emergent property of population-level analysis. While we did observe a large proportion of arm-neutral units (Figure 4B), careful analysis of model structure revealed that arm-dedicated units drove the separation of arm-specific neural subspaces (Figure 7). This segregation was particularly pronounced during movement, thus reducing any concern that small movements of the non-selected arm had an impact on our results or conclusions.

Importantly, contralateral signals were more independent than ipsilateral ones – a larger proportion of contralateral modulation occurred in contra-dedicated units than the reverse case for ipsi- (Figure 5). This was not a surprising result, as contralateral bias in the functional organization of motor cortex has been clearly revealed by effects stroke (Hatem et al., 2016), lesion studies (Brinkman and Kuypers, 1973), and cortical stimulation (Penfield and Boldrey, 1937; Alagona et al., 2001; Montgomery et al., 2013). One candidate hypothesis for the presence of ipsilateral activity has been that it supplies its own independent control signal. There is some evidence that ipsilateral cortex plays an increased role in movement following hemispheric damage (Brinkman and Kuypers, 1973; Hummel and Cohen, 2006; Dancause, 2006; Wilkins et al., 2020), though not necessarily a beneficial or compensatory one. The magnitude of ipsilateral encoding also increases with the degree of movement complexity (Verstynen et al., 2005) and may involve spatially distinct neural populations (Ziemann et al., 1999; Chen et al., 2003). Anatomically, the corticospinal tract (CST) is almost entirely contralateral, and the effectiveness of the

ipsilateral component has been debated (Lacroix et al., 2004; Rosenzweig et al., 2009; Soteropoulos et al., 2011; Baker et al., 2015). Ipsilateral cortex may also exert its influence via connections made in the reticular formation (Alagona et al., 2001; Baker et al., 2015; Wilkins et al., 2020), which projects to ipsilateral spinal cord. These reticulospinal pathways may also be responsible for preparatory modulation of muscle spindles (Papaioannou and Dimitriou, 2020), which is relevant to the weak emergence of independent activity we observed during the Instruct phase. Our results showed a small amount of independent ipsilateral activity (monkey O more so than monkey W), with more of the ipsilateral signal coming from non-dedicated units (Figure 5). Thus, if the ipsilateral hemisphere provides any independent control signal, it is much weaker than the contralateral signal. Rather, our results suggest a role in bimanual coordination or higher-level processing, which we now discuss.

Bilateral signals and their role in motor control

Our study adds to a large body of existing work reporting activity related to both ipsi- and contralateral arms in the same single-units during preparation (Hoshi and Tanji, 2002; Cisek and Kalaska, 2003) and movement (Cisek and Kalaska, 2003; Ames and Churchland, 2019; Heming et al., 2019). The presence of these units implies some form of bilateral network or interhemispheric communication. Increases in excitability of homologous effectors during transcranial magnetic stimulation (TMS) (McMilan et al., 2006) and symmetric activation patterns in functional magnetic resonance imaging (fMRI) (Verstynen and Ivry, 2011; Diedrichsen et al., 2013) suggest that bilateral motor cortical circuits are organized with mirrored properties. Mirror activation and other forms of interhemispheric communication have been proposed to support intermanual skill transfer (Diedrichsen et al., 2013) or shaping of contralateral activity patterns during complex behavior (Verstynen et al., 2005). In the present study we have not directly compared directional tuning between ipsi- and contralateral arm movements, and therefore cannot speak directly to mirrored response properties. However, we did observe that the distributed component of bilateral signals existed within a shared subspace for the two arms (Figure 8). Mirror activity would necessarily reside in the same neural subspace for each arm, provided that subspace is linear, as all linear subspaces are invariant with respect to reflection. Our results are therefore consistent with functional hypotheses of ipsilateral cortex involving mirror symmetric activation.

Distinct bimanual encoding patterns in motor cortex have been observed in both human fMRI (Diedrichsen et al., 2013) and single-unit monkey studies (Donchin et al., 1998; Kazennikov et al., 1999). Surgical transection of the corpus callosum, the primary direct connection between hemispheres (Gazzaniga, 1989), disrupts typical spatial coupling and continuous synchronization of arm movements as well (Franz et al., 1996; Kennerly et al., 2002). These studies may suggest that bilaterally distributed networks facilitate bimanual coordination, a function historically attributed to the supplementary motor area (Brinkman, 1981). Our task involved unimanual movements, containing no component of coordination. However, the result that meaningful information coding existed within a shared subspace (Figure 8) is consistent with a role in coordination. Even during unimanual movements, one must coordinate bilateral drive to counter Coriolis forces acting on the opposite hemibody. We make limited claims on this hypothesis due to our simplified behavior, and stress that implicating a role in bimanual coordination does not simply mean revealing a shared substrate for signals of both limbs. Nonetheless, a bi-hemispheric network structure may underly computations for controlling the two arms as a unified plant (Welford, 1968). M1 has been implicated in multi-joint integration for voluntary movement and feedback control (Scott, 2003; Pruszynski et al., 2011). Bimanual behaviors have a similar task of

overcoming redundant degrees of freedom (Bernstein, 1967). Many patterns of behavior for each arm independently may help one achieve an action goal so long as cooperation of the two remains intact ('motor equivalence', Lashley, 1933). This lower-dimensional behavioral coordination space, sometimes called 'the uncontrolled manifold' (Scholz and Schoner, 1999), would likely have a similar neural manifold in which bilateral arm signals interact (for related discussion and review, see Swinnen and Wenderoth, 2004; Wiesendanger and Serrien, 2004; Diedrichsen et al., 2010). The distributed space that we report may reflect such a manifold.

A dynamical systems interpretation

One unified explanation for the two components identified in this study is that they reflect a computational (or "hidden") layer and an output layer for cortical processing. In this framework, the distributed signal would reflect a bilateral network that plays a supportive role in motor processing rather than direct output. The output itself would be represented by the localized signal. The idea that bilaterally distributed networks contribute to computations that do not directly represent the output has been previously proposed by Ames and Churchland (2019). Preparatory activity in motor areas reflects abstract features of action and may lack a strong contralateral bias (Hoshi and Tanji, 2002; Cisek and Kalaska, 2003). The distinctive lack of laterality in the distributed signal we observed is consistent with other reports of abstract preparatory responses. It played a relatively stronger role during preparation as well, since the localized component did not fully develop until movement. This aligns with reports that behaviorally specific features become more apparent in motor cortical signals during active behavior, including laterality (Shen and Alexander, 1997; Cisek and Kalaska, 2003).

From a dynamical systems perspective, bi-hemispheric circuitry underlying the distributed signal could serve to enforce internal dynamics of the overall population. Preparatory signals in pre- and primary motor cortex are thought to converge on an ideal population state, or initial condition, such that internal circuit dynamics will guide appropriate patterns of activity for the upcoming movement (Churchland et al., 2006; Shenoy et al., 2013; Li et al., 2016). In a rodent licking task, Li et al. (2015) showed that preparatory activity in premotor neurons projecting to other cortical areas lacked strong laterality, while those with descending output had a pronounced contralateral bias and became active closer to movement onset. They later showed that bilaterally distributed networks provide robustness to unilateral perturbation during preparation and hypothesized that the two hemispheres operate together to maintain the network state (Li et al., 2016). While we do not claim to present a clean dissociation like those done with cell-type specific methods, our results generally align with this form of network structure. In addition to setting the initial state, persistence of the distributed component during movement may reflect the ongoing dynamics of pattern generation (Shenoy et al., 2013; Sussillo et al., 2015).

Within this interpretation, the increasing localization of population activity would reflect emergence of descending output from the network and mirror the well-established laterality of anatomical pathways (Brinkman and Kuypers, 1973; Soteropoulos et al., 2011). It could also, at least in part, reflect a timing signal for transitioning the network from preparation to movement (Sussillo et al., 2015; Kaufman et al., 2016) while simultaneously specifying the selected effector. These roles are in apparent conflict with the observation that population signals begin to localize even prior to movement (Figure 5,6). If this localized component represents unilateral output, then at least some of that output must be involved in

movement-null processes. Indeed, preparatory modulation in spinal interneurons (Prut and Fetz, 1999; Fetz et al., 2002), H-reflex (Duque et al., 2010), and motor evoked potentials (Duque et al., 2010) has been observed. Cortical output may contribute to this modulation indirectly via pathways such as the reticulospinal tracts (Keizer and Kuypers, 1989; Buford and Davidson, 2004). Premotor areas make connections with both M1 and the spinal cord (Dum and Strick, 2002), and may therefore provide some corticospinal output during preparation or movement as well.

In summary, we present a parsimonious statistical description of how population activity spanning M1 and PMd specifies motor plans for a single arm and provides unilateral output. The two components that we have identified will be crucial for contextualizing current theory on bilateral motor cortical processing as well as designing future experiments that investigate the independence and interaction of signals across the hemispheres.

METHODS

Behavioral recordings and task

Kinematic data were collected using LED-based motion tracking of several points along each arm (Phasespace Inc, San Leandro, CA). 3D positions of each LED were sampled at 240Hz. Prior to offline analysis, these positions were smoothed using a cubic spline and smoothing parameter 0.005 (*cspaps* function – MATLAB). The most distal LED, located on the back side of each hand just below the wrist, was used for online endpoint feedback and all offline analysis.

Monkeys were trained to perform a variant of an instructed-delay reaching task (Figure 1B). Endpoint feedback of each arm and all visual stimuli were presented to the animal using a custom-built virtual reality 3D display. This display consisted of two mirrors that projected shifted images independently to each eye to produce stereopsis. Cursors, indicating effector endpoint position, were color coded for the left (yellow) and right (purple) hands, as were all associated stimuli.

Each trial began with the appearance of the start positions for each hand (spherical targets, radius 4cm), located near the body on top of a physical bar that the monkey rested its hands on (Figure 1A). In a self-initiated manner, the monkey would assume the start position by placing both cursors in their appropriate starting positions and maintaining that position for 500 ms ('Rest' phase). Our threshold for detecting movement online was 9cm/s; breaking this threshold would abort the trial.

Marking the beginning of the 'Instruct' phase, a cue (spherical target, radius 3cm) would appear at one of six locations within a fronto-parallel plane 8cm in front of the start positions (Figure 1A). The color of the cue indicated the required arm, and position of the cue was the target location for the forthcoming reach. The instruction cue remained visible through the delay period, a duration that was sampled uniformly on the interval 500-1500ms. Movement beyond the speed threshold with either hand would abort the trial.

At the end of this period, two simultaneous changes signaled the monkey to move and marked the start of the 'Move' phase. First, the sphere defining the start position for the cued arm disappeared. Second, the cue at the target location enlarged (3cm to 4cm radius). The monkey then reached toward the target and once at the terminal location, had to maintain that position for 250ms. To earn a juice reward, the

animal had to initiate the reach within 500ms of the onset of the imperative, terminate the movement within the target's circumference, and keep the non-reaching hand stationary for the duration of the trial. To further emphasize that the trial was successful, the target turned green.

300ms windows were used to represent each phase in data analysis. For the Rest phase, we used the final 300ms before the onset of the instruction cue. For the Instruct phase, we used data in the interval between 200ms to 500ms post-cue. For the Move phase, we used the first 300ms following the onset of movement, defined as when speed of the reaching hand exceeded 10cm/s. We used a late window for the Rest phase to avoid any residual activity associated with moving to the start positions. The steady state neural response was used to position the Instruct phase window; this was reached approximately 200ms after the onset of the instruction cue (see Figure 7B). The Move window was selected to capture peak neural activity associated with movement while including only the feed-forward portion, which typically lasted 250-300ms (Figure 1C, bottom row). Reach durations were calculated as the time between movement onset and the first point where (1) movement speed dropped below 20cm/s, and (2) velocity in the depth direction reached 0.

Surgical implantation

All procedures were conducted in compliance with the National Institutes of Health Guide for the Care and Use of Laboratory Animals and were approved by the University of California at Berkeley Institutional Animal Care and Use Committee. Two adult male rhesus monkeys (Macaca mulatta) were implanted bilaterally with custom acute recording chambers (Grey Matter Research LLC, Bozeman, MT). Partial craniotomies within the chambers allowed access to the arm regions of dorsal premotor (PMd) and primary motor (M1) cortices in both hemispheres. Localization of target areas was performed using stereotactically aligned structural MRI collected just prior to implantation, alongside a neuroanatomical atlas of the rhesus brain (Paxinos et al, 2000).

Electrophysiology

Unit activity was collected using 24-32 channel multi-site probes (V-probe - Plexon Inc, Dallas, TX), with contacts separated by 100um and positioned axially along a single shank. Probes were lowered deep enough to cover roughly the full laminar structure of cortex (Figure 2B-C). The depth of insertion was determined by (1) measurements of the dural surface prior to recording, and (2) presence of spiking activity across all channels. 2 probes were typically inserted in each hemisphere daily and removed at the end of the session, one in PMd and one in M1. A total of 12 insertion points across PMd and M1 of each hemisphere were used across 13 recording sessions in Monkey O, and 6 insertion points across 7 sessions for Monkey W (Figure 2A).

Neural data were recorded using the OmniPlex Neural Recording Data Acquisition System (Plexon Inc, Dallas, TX). Spike sorting was performed offline (Offline Sorter – Plexon Inc, Dallas, TX). Single-unit waveforms were isolated in multi-dimensional feature space (including principal components, non-linear energy, waveform amplitudes) and rejected if either (1) the waveform clusters were not stable over the course of the session, or (2) >0.4% of inter-spike-intervals were below 1ms. For population level analyses (PCA, LDA), a small number of multi-units were included. A multi-unit was defined by waveform clusters that separated from the noise cluster and were stable over time, but did not quite meet the

inter-spike-interval criteria or contained what might be multiple unit clusters that could not be easily separated. For monkey O, the average proportion of multi-units in each single session population sample was 17%, ranging 12-25%. For monkey W, average 20%, ranging 12-32%.

Spiking data were binned in 20ms non-overlapping bins, square-root transformed to stabilize variance, and smoothed with a 50ms gaussian kernel for all analyses (Yu et al., 2009).

Modulation and Arm Preference metrics

Modulation was calculated as:

$$M = \left(\frac{x_t - \mu_{rest}}{\sigma_{rest} + 1}\right)^2,$$

where

$$x_t : instantaneous\ firing\ rate$$
$$\mu_{rest} : mean\ firing\ rate\ during\ Rest$$
$$\sigma_{rest} : standard\ deviation\ during\ Rest$$

This unitless metric reflects the deviation from baseline activity, normalized by baseline fluctuations. It may be thought of as a signal-to-noise ratio and is similar in form to variance when the mean is taken over a time window. The constant 1 was added to the denominator for soft-normalization to ensure that units which were silent during rest did not have exploding values and were not overly emphasized in the dataset. Because some units had slightly different activity on left and right arm trials even before instruction, the standard deviation during Rest was calculated separately for each arm and σ_{rest} was calculated as the mean of the two.

Arm Preference was calculated as:

$$AP = \frac{M_{contra} - M_{ipsi}}{M_{contra} + M_{ipsi}}$$

An arm preference of 1 corresponds to a unit that is exclusively modulated during contralateral trials, while an arm preference of -1 is the same for ipsilateral trials. Arm preferences were independently assigned for each phase of the task. In analyses that used arm preference along with other features, independent datasets were used to calculate each to avoid any mathematical coupling, since modulation itself is used in the arm preference calculation. Note also that the scaling factor used in the modulation calculation cancels out of the arm preference calculation, making it invariant to the choice of normalization.

Principal components analysis

Principal components analysis (PCA) was used to identify low-dimensional representations of population activity with the *pca* function in MATLAB. PCA computes an orthogonal basis set that reflects the principal axes of variation in the data. Individual components do not strictly correspond to observed activity patterns, and one should be wary of interpreting them as such, yet the low-dimensional space spanned by the top few components has been repeatedly used in systems neuroscience as a helpful

descriptor of coordinated ensemble activity (Cunningham and Yu, 2014). PCA was selected over other dimensionality reduction techniques for its widespread use and relative lack of assumptions.

Prior to fitting the models, firing rate data were soft-normalized using the same method as in the modulation strength calculation:

$$z_t = \frac{x_t - \mu_{rest}}{\sigma_{rest} + 1}$$

An alternative normalization factor was used to create Figure S2, replacing the denominator by the full firing rate range + 5Hz (Elsayed et al., 2016; Ames and Churchland, 2019; Heming et al., 2019). Since Rest phase mean activity was already subtracted from individual units, we did not de-mean again prior to computing PCA models. Measures of variance accounted for were not inflated by capturing means because they were computed using the variance of the component scores (Figure 7,8F):

$$V = Tr\big(Cov(XP)\big)$$

Where X is a $t\ x\ n$ data matrix and P is an $n\ x\ p$ projection matrix, given t time samples, n units, and p principal component dimensions.

Cross-validation approaches were used for all analyses and figures to address overfitting. This provided accurate and generalizable estimates of variance capturing metrics that could also be appropriately compared across datasets (i.e. across time or arms).

<u>Dimensionality estimation</u>

Dimensionality of the PCA subspace was estimated by optimizing the cross-validated reconstruction of full-dimensional neural data from component scores. Given *m* trials and *n* units, the following procedure was used:

1. Leave out the *i*th trial from the data matrix, yielding training data, $X^{(-i)}$, and testing data, $X^{(i)}$

2. Train PCA model of dimension $p < n$ on $X^{(-i)}$, using singular value decomposition (SVD) to compute the projection matrix, $P^{(-i)}$

3. Leave out the *j*th unit from the testing data and projection matrix by removing the *j*th column and row from each, respectively, yielding $X_{-j}^{(i)}$ and $P_{-j}^{(-i)}$

4. Using the Moore-Penrose pseudoinverse, find a new projection matrix with the *j*th unit removed, whose transpose is $\left(P_{-j}^{(-i)}\right)^{+}$

5. Calculate the component score for the *i*th trial using the remaining units and the new projection matrix, then estimate the *j*th unit from that component score by projecting back into the ambient space. As a single step, this calculation is:

$$\hat{X}_j^{(i)} = \left[P^{(-i)}\left(P_{-j}^{(-i)}\right)^{+}\left(X_{-j}^{(i)}\right)^{T}\right]_j$$

7. Repeat for trials *i*=1,…,*m* and units *j*=1,…,*n*

8. Repeat for component numbers *p*=1,…,*n*. Take the number of components that minimizes the predicted residual error sum of squares (PRESS) statistic:

$$PRESS = \sum_{i=1}^{m}\sum_{j=1}^{n}\left(X_j^{(i)} - \hat{X}_j^{(i)}\right)^2$$

This method provides estimates of the full-dimensional neural data, independent of the training set, by identifying consistent population structure. Similar methods have been used previously for assessing dimensionality reduction techniques for neural data (Yu et al., 2009). There are no mathematical constraints favoring increased dimensionality. As such, the dimensionality estimate is conservative and robust to overfitting. Using heuristics, such as the number of components to explain 90% variance, would be inappropriate for our analyses. They are prone to overfitting, which would include meaningless components and impair analysis of model structure via coefficient weights.

Covariance alignment

We computed a measure of similarity between pairs of subspaces that we call Covariance Alignment. Our method is essentially the same as that previously used for comparing low-dimensional spaces via factor analysis (Athalye et al., 2017). In short, this measure computes the proportion of low-dimensional variance from one dataset that is also captured in the low-dimensional space of another dataset.

Given $t\ x\ n$ data matrices X_A, X_B , where *n* is the number of units and *t* is the number of time samples, the following procedure was used:

1. Train PCA models of dimension $p < n$ on X_A and X_B, using SVD to compute the $n\ x\ p$ projection matrices, P_A and P_B

2. Project X_A into its own *p*-dimensional space and compute the variance as:

$$V_A = Tr\big(Cov(X_A P_A)\big) = Tr\big(Cov(T_A)\big)$$

3. Project the *p*-dimensional representation of X_A, which is T_A, into the *p*-dimensional space identified using X_B and compute the variance as:

$$V_{A\_in\_B} = Tr\big(Cov(X_A P_A P_A^T P_B)\big) = Tr\left(Cov(T_A P_A^T P_B)\right)$$

4. Return the proportion of *p*-dimensional variance from dataset *A* that is also captured in dataset *B*'s subspace using the ratio:

$$CA = \frac{V_{A\_in\_B}}{V_A} = \frac{Tr\big(Cov(X_A P_A P_A^T P_B)\big)}{Tr\big(Cov(X_A P_A)\big)} = \frac{Tr\big(Cov(T_A P_A^T P_B)\big)}{Tr\big(Cov(T_A)\big)}$$

This metric is subtly different from the alignment indices used in Elsayed et al., 2016 and Heming, Cross et al., 2019. The key difference here is the double projection in the numerator, which means that we are specifically capturing the proportion of low-dimensional variance from one dataset that is captured in the low-dimensional space of another, rather than the ratio of overall variance captured in two different subspaces.

802 PCA coefficient analysis

803 Since components of PCA models form an orthogonal basis set, each was independently analyzed to
804 determine its contribution to subspace divergence. Two statistics were calculated for each component
805 using held-out datasets.

806 First, we projected activity during trials of each arm onto a single component, calculated the variance of
807 the projections for each arm, and expressed them as a ratio. This captured each component's
808 contribution to discrimination between the arms. For component C, this calculation is:

809 $$V_{C,R/L} = \frac{Var(X_R P_C)}{Var(X_L P_C)}$$

810 Where X_R, X_L are $t\ x\ n$ data matrices for the right and left arms, respectively, and P_C is the $n\ x\ 1$
811 projection matrix for component C. The log of this ratio will be far from 0 if there is much more variance
812 for one arm than the other along the axis defined by P_C.

813 Second, we calculated a coefficient-weighted average of the arm preferences for all units. If non-zero
814 weights were only given to right arm dedicated units, this value would be 1; if weights were evenly
815 distributed across the spectrum of arm-preferences, this value would be 0. Therefore, this measure
816 captured the dependence of a given component on arm-dedicated units. The coefficient-weighted arm
817 preference, CAP, for component C was calculated as

818 $$CAP_C = \frac{A|P_C|}{\sum_{i=1}^{n} |P_{C,i}|}$$

819 Where A is the $1\ x\ n$ vector of arm preferences for each unit.

820

821 Linear discriminant analysis

822 Population coding of movement was analyzed using Linear Discriminant Analysis (LDA) with the *fitdiscr*
823 function in MATLAB. LDA assumes that each class (target x limb combination) is associated with a
824 multivariate normal distribution over the predictor variables (spiking activity of multiple units) having
825 identical covariance but different means. Uniform priors were enforced for all models. As it was
826 expected that the covariance may change across use of the two arms during reaching, LDA models were
827 trained separately for each limb to allow fitting of arm-specific covariance matrices. LDA was chosen for
828 its robustness to violations of the given assumptions and its history of success with neural data
829 (Diedrichsen et al., 2013; Rich and Wallis, 2016).

830

831 Fine timescale analysis of population coding and subspace development (heatmaps)

832 The same basic method was used for displaying fine timescale changes in population coding of
833 movements (via LDA) and covariance structure (via PCA, Covariance Alignment). Neural data were
834 organized as 3D tensors (units, time windows, trials). Comparisons were made between all possible pairs
835 of time windows, using fully independent trial sets to prevent overfitting. For LDA models, this consisted
836 of leave-one-out cross-validation; for Covariance Alignment, random partitioning into two datasets of
837 equal trial numbers. Averages of the cross-validated results provided the 2D matrices visualized using
838 heatmaps in Figure 6B-C and Figure 8C-D. A single row or column therefore reflects the similarity of

839 population coding or covariance between a single timepoint and all other timepoints across the trial.
840 Block diagonal structure in the heatmaps reveals locally consistent structure within task phases.

841

842 Permutation testing procedures
843 Permutation tests were used for both single and multi-factorial hypothesis testing when parametric
844 tests were inappropriate. Null distributions were constructed by constraining permutations to only data
845 that were exchangeable under the null hypothesis (Anderson and Braak, 2002). For example, we
846 maintained the crossed structure of Phase (Rest, Instruct, Move), by only permuting Phase labels within
847 units. 10,000 permutations were used for all analyses, and p-values were estimated as the proportion of
848 permutations resulting in test statistics that were at least as extreme as what was observed. In cases
849 where the observed test statistic was more extreme than any permutations, we assigned a p-value of
850 1/number of permutations = 1.0e-4.

851

SUPPLEMENTARY FIGURES

		Significantly modulated					
		Instruct			Move		
	Number SU's	Ipsi	Bi	Contra	Ipsi	Bi	Contra
PMd	433	68(16%)	154(36%)	105(24%)	52(12%)	245(57%)	94(22%)
	113	11(10%)	31(27%)	26(23%)	19(17%)	42(37%)	21(19%)
M1	331	57(17%)	95(29%)	61(18%)	47(14%)	194(59%)	60(18%)
	289	39(13%)	35(12%)	59(20%)	22(8%)	110(38%)	87(30%)

Table S1. Proportions of significantly modulated single-units across task phases.
For well isolated single-units in each brain area, the proportions of the total population that were significantly modulated when compared with the Rest phase (two-sample t-test, $p<0.05$). For each phase, single-units were classified as uniquely ipsi, contra, or bilaterally modulated. Top row in each pair of rows represents Monkey O, bottom row Monkey W.

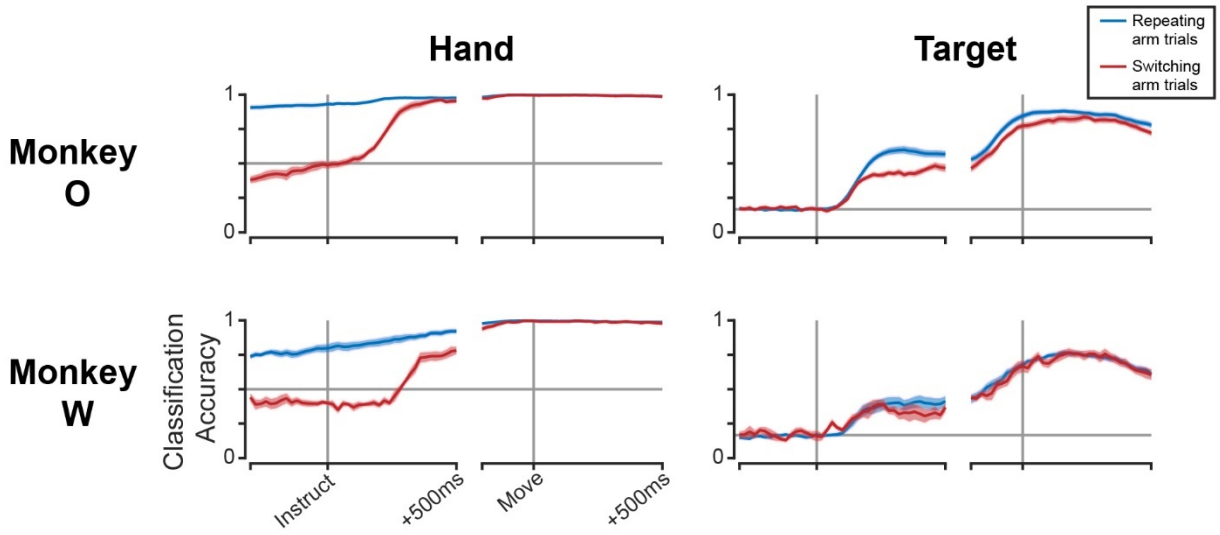

Figure S1. Arm-specific neural patterns exist during Rest on predictable trials.
Cross-validated classification accuracy for hand (left column) and target (right column) assignments. LDA models were trained on only trials that required use of the same arm as the previous trial, then tested on either held-out repeating arm trials (blue lines) or switching arm trials (red lines). Separate models were used for each timepoint. Horizontal grey lines indicate chance level. 13 Sessions for monkey O (top row); 7 sessions for monkey W (bottom row). Mean +/- standard error across sessions.

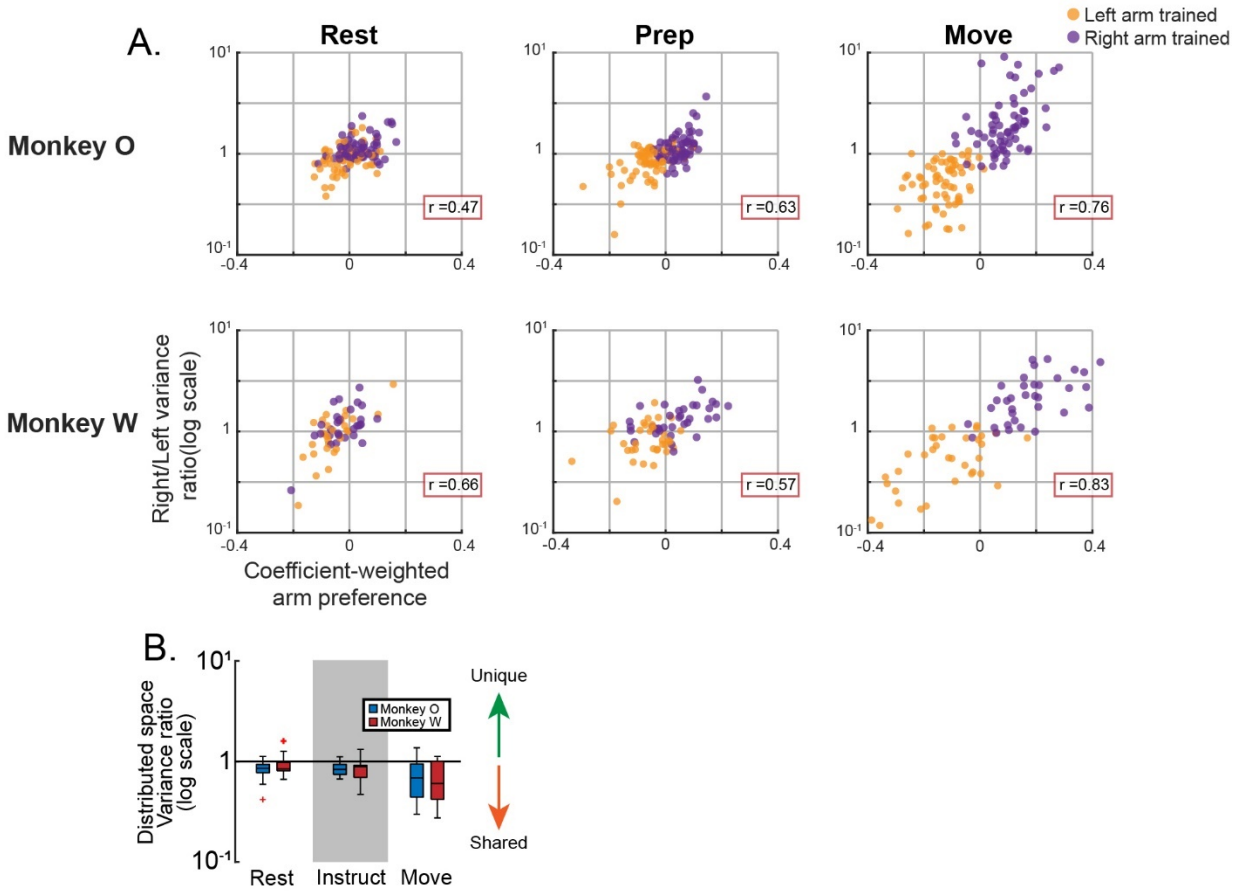

Figure S2. Subspace results using alternative firing rate normalization.
Prior to performing PCA, an alternative method of normalizing firing rates was used for these plots. Rather than dividing by the standard deviation at Rest, each unit's firing rate trace was divided by the full firing rate range + 5Hz (Elsayed et al., 2016; Ames and Churchland, 2019; Heming et al., 2019). This will mitigate the effect of highly modulated units, which PCA will preferentially represent otherwise. (A) Repetition of Figure 7D. (B) Repetition of Figure 8F.

ACKNOWLEDGEMENTS

We thank M. Kitano for help in NHP care and handling, and A. You, W. Liberti and Z. Balewski for helpful discussions. This work was supported by the National Defense Science and Engineering Graduate Fellowship to T.C.D, and a grant from the National Institute of Health (NS097480) to J.M.C.

COMPETING INTERESTS

We declare no competing interests.

AUTHOR CONTRIBUTIONS

T.C.D., C.M.M., R.B.I., and J.M.C. conceived and designed the experiments. T.C.D. performed the experiments, analyzed the data, and wrote the manuscript. T.C.D., C.M.M., J.D.W., R.B.I., and J.M.C reviewed and edited the manuscript.

REFERENCES

1. Alagona G, Delvaux V, Gérard P, De Pasqua V, Pennisi G, Delwaide PJ, Nicoletti F, Maertens De Noordhout A. 2001. Ipsilateral motor responses to focal transcranial magnetic stimulation in healthy subjects and acute-stroke patients. *Stroke*, *32*(6), 1304–1309. https://doi.org/10.1161/01.STR.32.6.1304
2. Ames KC, Churchland MM. 2019. Motor cortex signals for each arm are mixed across hemispheres and neurons yet partitioned within the population response. *eLife*, *8*, 1–36. https://doi.org/10.7554/eLife.46159
3. Anderson M, ter Braak CJF. 2002. Permutation tests for multi-factorial analysis of variance. *Journal of Statistical Computation and Simulation*, *73*(2), 85–113.
4. Athalye VR, Costa RM, Ganguly K, Costa RM, Carmena JM. 2017. Emergence of Coordinated Neural Dynamics Underlies Neuroprosthetic Learning and Skillful Control. *Neuron*, *93*(4), 955-970.e5. https://doi.org/10.1016/j.neuron.2017.01.016
5. Baker SN, Zaaimi B, Fisher KM, Edgley SA, Soteropoulos DS. 2015. Pathways mediating functional recovery. *Progress in Brain Research* (1st ed., Vol. 218). Elsevier B.V. https://doi.org/10.1016/bs.pbr.2014.12.010
6. Bernstein NA. 1967. The Co-ordination and Regulation of Movements. Pergamon Press, Oxford.
7. Brinkman C. 1981. Lesions in supplementary motor area interfere with a monkey's performance of a bimanual coordination task. *Neuroscience Letters*, *27*(3), 267–270. https://doi.org/10.1016/0304-3940(81)90441-9
8. Brinkman J, Kuypers HGJM. 1973. Cerebral control of contralateral and ipsilateral arm, hand and finger movements in the split brain rhesus monkey. *Brain*, *93*, 653–674. PubMed: 4204228
9. Buford, J. A., & Davidson, A. G. (2004). Movement-related and preparatory activity in the reticulospinal system of the monkey. *Experimental Brain Research*, *159*(3), 284–300. https://doi.org/10.1007/s00221-004-1956-4

10. Calabrese E, Badea A, Coe CL, Lubach GR, Shi Y, Styner MA, Johnson A. 2015. A diffusion tensor MRI atlas of the postmortem rhesus macaque brain. *Neuroimage* 117:408–416. https://doi.org/10.1016/j.neuroimage.2015.05.072
11. Carmena JM, Lebedev MA, Crist RE, O'Doherty JE, Santucci DM, Dimitrov DF, Patil PG, Henriquez CS, Nicolelis MAL. 2003. Learning to control a brain-machine interface for reaching and grasping by primates. *PLoS Biology*, *1*(2), 193–208. https://doi.org/10.1371/journal.pbio.0000042
12. Chen R, Yung D, Li JY. 2003. Organization of ipsilateral excitatory and inhibitory pathways in the human motor cortex. *Journal of Neurophysiology*, *89*(3), 1256–1264. https://doi.org/10.1152/jn.00950.2002
13. Churchland MM, Yu BM, Ryu SI, Santhanam G, Shenoy KV. 2006. Neural Variability in Premotor Cortex Provides a Signature of Motor Preparation. *Journal of Neuroscience*, *26*(14), 3697–3712. https://doi.org/10.1523/JNEUROSCI.3762-05.2006
14. Churchland MM, Cunningham JP, Kaufman MT, Ryu SI, Shenoy KV. 2010. Cortical Preparatory Activity: Representation of Movement or First Cog in a Dynamical Machine? *Neuron*, *68*(3), 387–400. https://doi.org/10.1016/j.neuron.2010.09.015
15. Churchland MM, Cunningham JP, Kaufman MT, Foster JD, Nuyujukian P, Ryu SI, Shenoy KV. 2012. Neural Population Dynamics During Reaching. *Nature*, *487*(7405), 1–20. https://doi.org/10.1016/j.micinf.2011.07.011.Innate
16. Cisek P, Crammond DJ, Kalaska JF. 2003. Neural activity in primary motor and dorsal premotor cortex in reaching tasks with the contralateral versus ipsilateral arm. *J Neurophysiol, 89*(2), 922-942.
17. Cunningham JP, Yu BM. 2014. Dimensionality reduction for large-scale neural recordings. *Nature Neuroscience*, *17*(11), 1500–1509. https://doi.org/10.1038/nn.3776
18. Dancause N. 2006. Vicarious function of remote cortex following stroke: Recent evidence from human and animal studies. *Neuroscientist*, *12*(6), 489–499. https://doi.org/10.1177/1073858406292782
19. Diedrichsen J, Shadmehr R, Ivry RB. 2010. The coordination of movement: optimal feedback control and beyond. *Trends in Cognitive Sciences*, *14*(1), 31–39. https://doi.org/10.1016/j.tics.2009.11.004
20. Diedrichsen J, Wiestler T, Krakauer JW. 2013. Two distinct ipsilateral cortical representations for individuated finger movements. *Cerebral Cortex*, *23*(6), 1362–1377. https://doi.org/10.1093/cercor/bhs120
21. Donchin O, Gribova A, Steinberg O, Bergman H, Vaadia E. 1998. Primary motor cortex is involved in bimanual coordination. *Nature, 395*(6699), 274-278.
22. Dum R, Strick P. 2002. Motor Areas in the Frontal Lobe, *77*, 677–682. https://doi.org/10.1201/9780203503584.sec1
23. Duque J, Lew D, Mazzocchio R, Olivier E, Ivry RB. 2010. Evidence for Two Concurrent Inhibitory Mechanisms during Response Preparation. *Journal of Neuroscience*, *30*(10), 3793–3802. https://doi.org/10.1523/JNEUROSCI.5722-09.2010
24. Elsayed GF, Lara AH, Kaufman MT, Churchland MM, Cunningham JP. 2016. Reorganization between preparatory and movement population responses in motor cortex. *Nature Communications*, 13239. https://doi.org/10.1038/ncomms13239
25. Fetz EE, Perlmutter SI, Prut Y, Seki K, Votaw S. 2002. Roles of primate spinal interneurons in preparation and execution of voluntary hand movement. *Brain Research Reviews*, *40*(1–3), 53–65. https://doi.org/10.1016/S0165-0173(02)00188-1
26. Franz EA, Eliassen JC, Ivry RB, Gazzaniga MS. 1996. Dissociation of spatial and temporal coupling in the bimanual movements of callosotomy patients. *Psychological Science*, *16*(2), 60–61. https://doi.org/10.1111/j.1467-9639.1994.tb00691.x

27. Ganguly K, Secundo L, Ranade G, Orsborn A, Chang EF, Dimitrov DF, Wallis JD, Barbaro NM, Knight RT, Carmena JM. 2009. Cortical representation of ipsilateral arm movements in monkey and man, *27*(52), 14299–14307. https://doi.org/10.1523/JNEUROSCI.3593-07.2007.Omega-3
28. Gazzaniga MS. 1989. Organization of the human brain. *Science*, *245*(4921), 947 LP – 952. https://doi.org/10.1126/science.2672334
29. Hatem SM, Saussez G, della Faille M, Prist V, Zhang X, Dispa D, Bleyenheuft Y. 2016. Rehabilitation of motor function after stroke: A multiple systematic review focused on techniques to stimulate upper extremity recovery. *Frontiers in Human Neuroscience*, *10*(SEP2016), 1–22. https://doi.org/10.3389/fnhum.2016.00442
30. Heming EA, Cross KP, Takei T, Cook DJ, Scott SH. 2019. Independent representations of ipsilateral and contralateral limbs in primary motor cortex. *ELife*, *8*(2002), 1–26. https://doi.org/10.7554/eLife.48190
31. Hoshi E, Tanji J. 2002. Contrasting neuronal activity in the dorsal and ventral premotor areas during preparation to reach. *Journal of Neurophysiology*, *87*(2), 1123–1128. https://doi.org/10.1152/jn.00496.2001
32. Hummel, F. C., & Cohen, L. G. (2006). Non-invasive brain stimulation: a new strategy to improve neurorehabilitation after stroke? *The Lancet Neurology*, *5*(8), 708–712.
33. Jankowska E, Cabaj A, Pettersson, LG. 2005. How to enhance ipsilateral actions of pyramidal tract neurons. *Journal of Neuroscience*, *25*(32), 7401–7405. https://doi.org/10.1523/JNEUROSCI.1838-05.2005
34. Kaufman MT, Churchland MM, Ryu SI, Shenoy KV. 2014. Cortical activity in the null space: Permitting preparation without movement. *Nature Neuroscience*, *17*(3), 440–448. https://doi.org/10.1038/nn.3643
35. Kaufman MT, Seely JS, Sussillo D, Ryu SI, Shenoy KV, Churchland MM. 2016. The largest response component in the motor cortex reflects movement timing but not movement type. ENeuro, 3(4). https://doi.org/10.1523/ENEURO.0085-16.2016
36. Kazennikov O, Hyland B, Corboz M, Babalian A, Rouiller EM, Wiesendanger M. 1999. Neural activity of supplementary and primary motor areas in monkeys and its relation to bimanual and unimanual movement sequences. *Neuroscience*, *89*(3), 661–674. https://doi.org/10.1016/S0306-4522(98)00348-0
37. Keizer K, Kuypers HGJM. 1989. Distribution of corticospinal neurons with collaterals to the lower brain stem reticular formation in monkey (Macaca fascicularis). *Experimental Brain Research*, 311–318.
38. Kennerley SW, Diedrichsen J, Hazeltine E, Semjen A, Ivry RB. 2002. Callosotomy patients exhibit temporal uncoupling during continuous bimanual movements. *Nature Neuroscience*, *5*(4), 376–381. https://doi.org/10.1038/nn822
39. Lacroix S, Havton LA, McKay H, Yang H, Brant A, Roberts J, Tuszynski MH. 2004. Bilateral Corticospinal Projections Arise from Each Motor Cortex in the Macaque Monkey: A Quantitative Study. *Journal of Comparative Neurology*, *473*(2), 147–161. https://doi.org/10.1002/cne.20051
40. Lashley KS. 1933. Integrative functions of the cerebral cortex. Physiol. Rev., 13: 1–42.
41. Lawrence DG, Kuypers HGJM. 1968. The Functional Organization of the Motor System in the Monkey. *Brain*, *91*(1), 15–36. https://doi.org/10.1093/brain/91.1.15
42. Li N, Chen T, Guo ZV, Gerfen CR, Svoboda K. 2015. A motor cortex circuit for motor planning and movement. *Nature*, *519*(7541), 51–56. https://doi.org/10.1038/nature14178
43. Li N, Daie K, Svoboda K, Druckmann S. 2016. Robust neuronal dynamics in premotor cortex during motor planning. *Nature*, *537*(7618), 122. https://doi.org/10.1038/nature18623

44. Matsunami K, Hamada I. 1981. Characteristics of the ipsilateral movement-related neuron in the motor cortex of the monkey. *Brain Research*, *204*(1), 29–42. https://doi.org/10.1016/0006-8993(81)90649-1
45. Maxwell DJ, Soteropoulos DS. 2019. The mammalian spinal commissural system: properties and functions. *Journal of Neurophysiology*, *123*(1), 4–21. https://doi.org/10.1152/jn.00347.2019
46. McMillan S, Ivry RB, Byblow WD. 2006. Corticomotor excitability during a choice-hand reaction time task. *Exp Brain Res, 172*(2), 230-245.
47. Montgomery LR, Herbert WJ, Buford JA. 2013. Recruitment of ipsilateral and contralateral upper limb muscles following stimulation of the cortical motor areas in the monkey. *Experimental Brain Research*, *230*(2), 153–164. https://doi.org/10.1007/s00221-013-3639-5
48. Noskin O, Krakauer JW, Lazar RM, Festa JR, Handy C, O'Brien KA, Marshall RS. 2008. Ipsilateral motor dysfunction from unilateral stroke: implications for the functional neuroanatomy of hemiparesis. *J Neurol Neurosurg Psychiatry, 79*(4), 401-406.
49. Papaioannou S, Dimitriou M. 2020. Goal-dependent tuning of muscle spindle receptors during movement preparation. *bioRxiv*. https://doi.org/10.1101/2020.03.06.981530
50. Paxinos G, Huang XF, Toga AW. 2000. The Rhesus Monkey Brain in Stereotaxic Coordinates. Academic Press.
51. Penfield W, Boldrey E. 1937. Somatic motor and sensory representation in the cerebral cortex of man as studied by electrical stimulation. *Brain*, 389–443. https://doi.org/10.1093/brain/60.4.389
52. Pruszynski JA, Kurtze I, Nashed JY, Omrani M, Brouwer B, Scott SH. 2011. Primary motor cortex underlies multi-joint integration for fast feedback control. *Nature*, *478*(7369), 387–390. https://doi.org/10.1038/nature10436
53. Rich E, Wallis JD. 2016. Decoding subjective decisions from orbitofrontal cortex supplementary. *Nature Neuroscience*, *19*(7), 973–980. https://doi.org/10.1038/nn.4320
54. Rosenzweig ES, Brock JH, Culbertson MD, Lu P, Moseanko R, Edgerton VR, Havton LA, Tuszynski MH. 2009. Extensive spinal decussation and bilateral termination of cervical corticospinal projections in rhesus monkeys. *J Comp Neurol, 513*(2), 151-163.
55. Scholz, J. P., & Schöner, G. (1999). The uncontrolled manifold concept: Identifying control variables for a functional task. *Experimental Brain Research*, *126*(3), 289–306. https://doi.org/10.1007/s002210050738
56. Scott, S. H. (2003). The role of primary motor cortex in goal-directed movements: Insights from neurophysiological studies on non-human primates. *Current Opinion in Neurobiology*, *13*(6), 671–677. https://doi.org/10.1016/j.conb.2003.10.012
57. Shen L, Alexander GE. 1997. Preferential representation of instructed target location versus limb trajectory in dorsal premotor area. *Journal of Neurophysiology*, *77*(3), 1195–1212. https://doi.org/10.1152/jn.1997.77.3.1195
58. Shenoy KV, Sahani M, Churchland, MM. 2013. Cortical Control of Arm Movements: A Dynamical Systems Perspective. *Annual Review of Neuroscience*, *36*(1), 337–359. https://doi.org/10.1146/annurev-neuro-062111-150509
59. Soteropoulos DS, Edgley SA, Baker, SN. 2011. Lack of evidence for direct corticospinal contributions to control of the ipsilateral forelimb in monkey. *Journal of Neuroscience*, *31*(31), 11208–11219. https://doi.org/10.1523/JNEUROSCI.0257-11.2011
60. Sussillo D, Churchland MM, Kaufman MT, Shenoy KV. 2015. A neural network that finds a naturalistic solution for the production of muscle activity. *Nat Neurosci*, *116*(8), 1477–1490. doi:10.1038/nn.4042

61. Swinnen, S. P., & Wenderoth, N. (2004). Two hands, one brain: Cognitive neuroscience of bimanual skill. *Trends in Cognitive Sciences*, *8*(1), 18–25. https://doi.org/10.1016/j.tics.2003.10.017
62. Tanji J, Okano K, Sato KC. 1988. Neuronal activity in cortical motor areas related to ipsilateral, contralateral, and bilateral digit movements of the monkey. *Journal of Neurophysiology*, *60*(1), 325–343. https://doi.org/10.1152/jn.1988.60.1.325
63. Verstynen T, Diedrichsen J, Albert N, Aparicio P, Ivry RB. 2005. Ipsilateral motor cortex activity during unimanual hand movements relates to task complexity. *J Neurophysiol, 93*(3), 1209-1222.
64. Verstynen T, Ivry RB. 2011. Network dynamics mediating ipsilateral motor cortex activity during unimanual actions. *Journal of Cognitive Neuroscience*, *23*(9), 2468–2480. https://doi.org/10.1162/jocn.2011.21612
65. Weinrich M, Wise SP, Mauritz KH. 1984. A neurophysiological study of the premotor cortex in the rhesus monkey. *Brain*, *107*(2), 385–414. https://doi.org/10.1093/brain/107.2.385
66. Welford AT. 1968. Fundamentals of Skill. Methuen, London.
67. Wiesendanger, M., & Serrien, D. J. (2004). The quest to understand bimanual coordination. *Progress in Brain Research*, *143*(03), 491–505. https://doi.org/10.1016/S0079-6123(03)43046-X
68. Wilkins KB, Yao J, Owen M, Karbasforoushan H, Carmona C, Dewald, JPA. 2020. Limited capacity for ipsilateral secondary motor areas to support hand function post-stroke. *Journal of Physiology*, *598*(11), 2153–2167. https://doi.org/10.1113/JP279377
69. Yu BM, Cunningham JP, Santhanam G, Ryu SI, Shenoy KV, Sahani M. 2009. Gaussian-process factor analysis for low-dimensional single-trial analysis of neural population activity. *Journal of Neurophysiology*, *102*(1), 614–635. https://doi.org/10.1152/jn.90941.2008
70. Ziemann U, Ishii K, Borgheresi A, Yaseen Z, Battaglia F, Hallett M, Cincotta M, Wassermann EM. 1999. Dissociation of the pathways mediating ipsilateral and contralateral motor-evoked potentials in human hand and arm muscles. *Journal of Physiology*, *518*(3), 895–906. https://doi.org/10.1111/j.1469-7793.1999.0895p.x